

54686

Armed Services Technical Information Agency

AD #54686

Reproduced by

DOCUMENT SERVICE CENTER

KNOTT BUILDING, DAYTON, 2, OHIO

Because of our limited supply, you are requested to
RETURN THIS COPY WHEN IT HAS SERVED YOUR PURPOSE
so that it may be made available to other requesters.
Your cooperation will be appreciated.

19990301068

NOTICE: WHEN GOVERNMENT OR OTHER DRAWINGS, SPECIFICATIONS OR OTHER DATA ARE REUSED FOR ANY PURPOSE OTHER THAN IN CONNECTION WITH A DEFINITELY RELATED GOVERNMENT PROCUREMENT OPERATION, THE U. S. GOVERNMENT THEREBY INCURS NO RESPONSIBILITY, NOR ANY OBLIGATION WHATSOEVER; AND THE FACT THAT THE GOVERNMENT MAY HAVE FORMULATED, FURNISHED, OR IN ANY WAY SUPPLIED THE SAID DRAWINGS, SPECIFICATIONS, OR OTHER DATA IS NOT TO BE REGARDED BY ANY APPLICATION OR OTHERWISE AS IN ANY MANNER LICENSING THE HOLDER OR ANY OTHER PERSON OR CORPORATION, OR CONVEYING ANY RIGHTS OR PERMISSION TO MANUFACTURE OR SELL ANY PATENTED INVENTION THAT MAY IN ANY WAY BE RELATED THERETO.

UNCLASSIFIED

REPRODUCTION QUALITY NOTICE

This document is the best quality available. The copy furnished to DTIC contained pages that may have the following quality problems:

- **Pages smaller or larger than normal.**
- **Pages with background color or light colored printing.**
- **Pages with small type or poor printing; and or**
- **Pages with continuous tone material or color photographs.**

Due to various output media available these conditions may or may not cause poor legibility in the microfiche or hardcopy output you receive.

If this block is checked, the copy furnished to DTIC contained pages with color printing, that when reproduced in Black and White, may change detail of the original copy.

~~AD#~~ 54686

CORNELL AERONAUTICAL LABORATORY, INC.

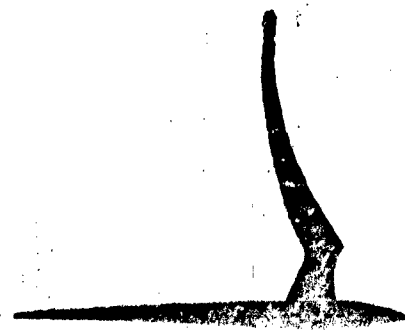
AD 54686

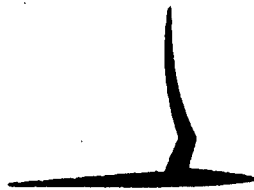
Final Report

AD NO. ASTIA FILE COPY

<p>REPORT NO. UB-909-D-1</p> <p>WIND TUNNEL TESTS OF A 1/24 SCALE MODEL AIR SUPPORTED RADOME AND TOWER</p> <p>J. S. Air Force Home Air Development Center</p> <p>Contract No. AF 30(602)-976 September 24, 1954</p> <p>Copy No. 7</p>

RADC T.R. 54-86





CORNELL AERONAUTICAL LABORATORY, INC.

BUFFALO, N. Y.

REPORT NO. UB-909-D-1

**WIND TUNNEL TESTS
OF A
1/24-SCALE MODEL AIR SUPPORTED RADOME AND TOWER**

CONTRACT NO. AF 30(602)-976

**U. S. AIR FORCE
ROME AIR DEVELOPMENT CENTER
GRIFFISS AIR FORCE BASE
ROME, NEW YORK**

By: Industrial Division

Date: Sept. 24, 1954

Prepared by:

Murray Kamrass

Murray Kamrass

approved by:

Walter W. Bird

Walter W. Bird, Asst. Head
Industrial Division

TABLE OF CONTENTS

	<u>Page</u>
<u>PART I</u>	
A. Purpose	1
1. Introduction	1
2. Problem Breakdown	1
B. General Factual Data	2
1. Identification of Technicians	2
2. Patents	2
3. References	3
4. Formulae	4
5. Measurement Procedures	12
C. Detail Factual Data	15
1. Model	15
2. Data - Comparison of Measured and Theoretical	19
3. Effect of Terrain	31
4. Effect of Reynolds' Number	31
5. Effect of Internal Pressure	33
6. Wind Tunnel Blockage Correction	33
7. Discussion	35
<u>PART II - Recommendations</u>	
A. Aerodynamic Loading of Radome	38
B. Tower Loading	38
1. Lift Loads	38
2. Drag Loads (Shear)	39
3. Radome Attachment Loads	40
C. Envelope Stresses	40
D. Required Inflation Pressure	40
E. Effect of Terrain	40

LIST OF ILLUSTRATIONS

<u>No.</u>	<u>Page</u>
Frontispiece	ii
1. Radome Geometry	4
2. Resolution of Forces	5
3. Tangent Diagrams	5
4. Mean Pressure Distributions	7
5. Lift Elements	8
6. Lift Distribution	9
7. Radome Side Elevation	10
8. Lift and Shear Beams	13
9. Schematic Diagram of Strain Gage Installation	14
10. Model Tower	16
11. Model Tower and Wedge	17
12. Balance System	18
13. Calculated Lift Loads	20
14a. Base Lift Loads	22
14b. Base Lift Loads	23
15. Base Shear Loads	25
16. Base Shear Distribution	26
17. Drag Distribution	28
18. Variation of Lift with Angle of Tilt	30
19. Effect of Reynolds' Number	32

P A R T I

A. PURPOSE

A-1. Introduction

A-1a. For the past six years, the design of air supported radomes and their supporting towers has been based on the recommendations outlined in the Design Manual for Spherical Air Supported Radomes (Ref. 1). This Manual was prepared using the classical pressure distribution around a sphere as a basis for the aerodynamic loading on the radome. This distribution was modified to take into account the effect of the base tower on the airflow across the radome. The theoretical calculations were also correlated with the limited amount of wind tunnel test data available in order to arrive at reasonable design values. Design recommendations based on these data were believed to be conservative and sufficiently accurate for design purposes, provided that recommended factors of safety were maintained.

A-1b. Recently, however, a need has arisen for radomes suitable for use in areas where wind velocities of 150 mph are likely to be encountered. The forces which such winds would impose on the radome envelope and tower are over 40% greater than those resulting from the 125 mph winds considered maximum at the time the Manual was prepared. More accurate data are thus required to insure an economical, yet adequate, structural design.

A-1c. It was decided that a wind tunnel program would be the optimum method of obtaining tower loading and other data required for design purposes. In order to obtain maximum value from the program it was decided that the effect of the following parameters should be investigated:

- (1) Wind speed (up to 200 mph)
- (2) Internal inflation pressure
- (3) Angle of attack (simulating a hilltop installation with wind sweeping up over the radome)
- (4) Reynolds' number (to determine, if possible, variation in lift or drag coefficient with Reynolds' number)

A-2. Problem Breakdown

A-2a. Design and Fabrication of Wind Tunnel Model: A 1/24-scale wind tunnel model was designed and fabricated, using a light weight two-ply, 45° bias constructed neoprene coated nylon envelope and a rigid plywood tower having a shape similar to the AN/FPS-6 arctic tower. The radome envelope was attached to a base angle, instrumented so that shear and tension loads acting on the tower could be measured. Pressure taps were installed in the radome envelope and tower so that pressure data could be obtained. Provision was made for controlling inflation pressure inside the radome. A more detailed description of the model is given in Part C of this report.

A-2b. Wind Tunnel Tests: The model was installed in the Cornell Aeronautical Laboratory twelve foot variable density wind tunnel. All pressure and electrical lines were connected and checked out. Five wind tunnel runs were made as follows:

- (1) Tower level, 1/2 atmosphere, velocity 50-200 miles per hour
- (2) Tower level, 1 atmosphere, velocity 50-200 miles per hour
- (3) Tower tilted 15 degrees, 1 atmosphere, velocity 50-200 miles per hour
- (4) Tower tilted 30 degrees, 1 atmosphere, velocity 50-200 miles per hour
- (5) Tower level, 1-1/2 atmospheres, velocity 50-175 miles per hour

A-2c. Calculation of Data and Final Report: Following the wind tunnel tests it was necessary to reduce the test data to a form suitable for comparison and presentation. This work included the calculation of strain gage loads, pressure coefficients, tunnel parameters, plotting of pressure data, calculation of theoretical loads to compare with strain gage data, etc. The results of these calculations are presented in Section C of this report.

B. GENERAL FACTUAL DATA

B-1. Identification of Technicians

The following individuals were the major technical contributors to this program. From time to time other engineers spent small amounts of time on the project, but these are not included below. Also not identified are the electronic and mechanical technicians and shop personnel whose work was done under the supervision of the listed personnel.

1. Bird, K. D.

R.P.I., B.S. in Aeronautical Engineering
1946-1947 Engineer, Aircraft Laboratory, Wright Field
1947-1951 Engineer, Applied Physics Lab., Johns Hopkins Univ.
1951-Pres. Head, Operating Section, Wind Tunnel Dept., Cornell Aeronautical Laboratory
Hours on this program - 9

2. Bird, W. W.

M.I.T., B.S. in Aeronautical Engineering
M.I.T., Fellow in Business and Engineering Administration
1934-1939, Engineer, Pullman Standard Car Mfg. Co.
1939-1945, Head of Eng. Lab., Curtiss Wright Corp.
1945-1946, Chief Test Engineer, Columbia Aircraft Corp.
1946-Pres. Asst. Dept. Head, Industrial Division, Cornell Aeronautical Laboratory
Hours on this program - 50

3. Czeck, E. A.

Aeronautical University (Chicago)
1951-1953 U. S. Navy, Aviation Metalsmith, 3rd class, and Airframe Engineer at Corpus Christie
1953-1954 Assistant Aeronautical Engineer, Wind Tunnel Dept., Cornell Aeronautical Laboratory
Hours on this program - 8

4. Kamrass, M.
Univ. of Mich., B.S. in Aeronautical Engineering
Univ. of Buffalo, M.S. in Mechanical Engineering
1942-1944, Aerodynamicist, Stinson Division, Consolidated
Vultee Aircraft Corp.
1944-1946, U. S. Army
1946-Pres. Research Engineer, Industrial Division, Cornell
Aeronautical Laboratory
Hours on this program - 460

5. Smith, M. D.
Clarkson College of Technology, Bachelor of Mechanical Eng.
1943-1950, Flight Test Instrumentation Engineer, Curtiss
Wright Corp.
1950-Pres. Research Engineer, Industrial Division, Cornell
Aeronautical Laboratory
Hours on this program - 115

6. Shoemaker, N.
Univ. of Florida, B.S. in Mechanical Engineering
1942-1946, U. S. Navy
1946-Pres. Associate Research Engineer, Industrial Division,
Cornell Aeronautical Laboratory
Hours on this program - 113

B-2. Patents

B-2a. No existing patents are applicable to the problem at hand.

B-2b. No patents are pending or inventions being considered for
patent.

B-3. References

1. Bird, Walter W., Design Manual for Spherical Air Supported
Radomes, Cornell Aeronautical Laboratory Report No. UB-664-D-1,
2 October 1950.
2. Dodge, R.A. and Thompson, M.J., Fluid Mechanics, McGraw Hill
Book Co., 1937.
3. Brand, L., Vector and Tensor Analysis, John Wiley & Sons, Inc.,
1948.
4. Streeter, V.L., Fluid Dynamics, McGraw Hill Book Co., Inc.,
1948.
5. Herriot, John G., Blockage Corrections for Three Dimensional
Flow Closed Throat Wind Tunnels, with Consideration of the
Effect of Compressibility, NACA Report 995, 1950.

B-4. Formulae

B-4a. Geometrical Symbols

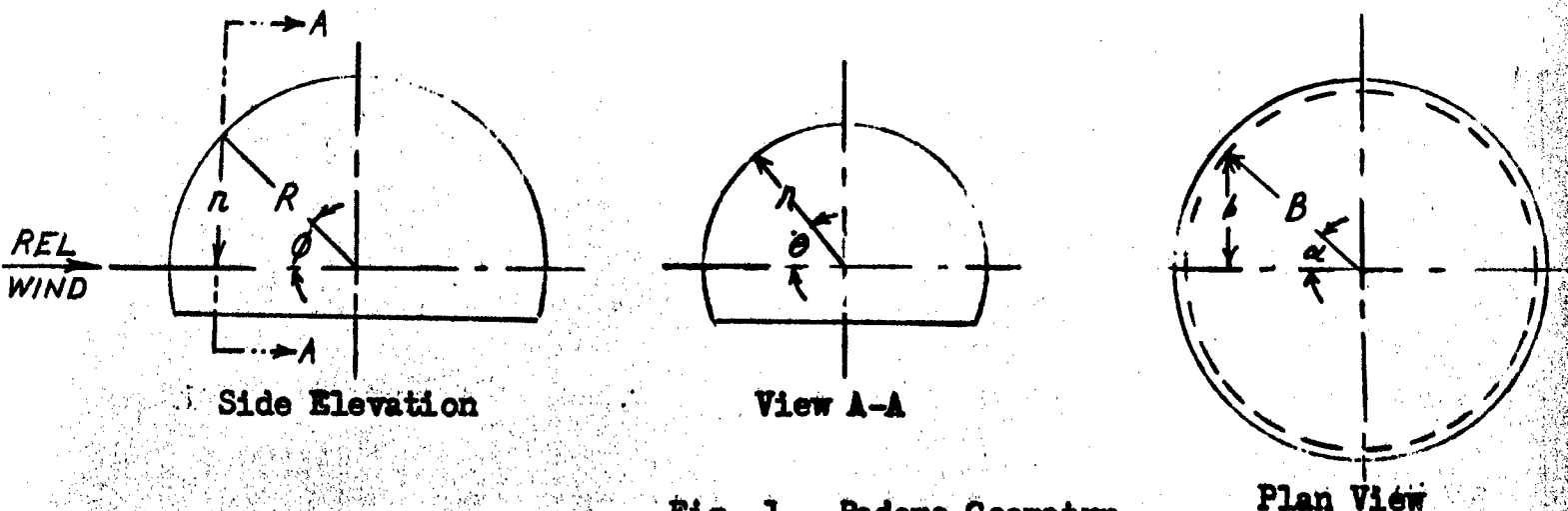


Fig. 1. Radome Geometry

- B Radius of base = 12.5 inches.
- b 1/2 length of intersection of base with plane of latitudinal circle.
- R Radius of sphere = 13.5 inches.
- r Radius of latitudinal circle.
- α Azimuth angle (from relative wind).
- β Base angle
- γ Angle between shear component and N_e . (See Fig. 2).
- θ Angle from horizontal plane through center of sphere.
- ϕ Angle from stagnation point on sphere
- ω Angle between tangents to the crown great circle and the latitudinal circle at the base (See Fig. 2).
- η Direction angle of tangent to radome surface (See Fig. 3).
- λ " " " " " "
- ν " " " " " "

B-4b. Other Symbols

- A Area
- D Drag
- d Drag of elemental area
- K Pressure coefficient = $\frac{p - p_{\infty}}{q}$
- K_D Drag coefficient
- K_L Lift coefficient
- L Lift
- N_N Fabric load along great circle through North Pole
- N_θ Fabric load in latitudinal direction
- N_ϕ Fabric load in longitudinal direction
- p_∞ Free stream static pressure
- q Dynamic pressure = $\rho U^2 / 2$
- S Shear force
- U Wind velocity
- x Ordinate in wind direction

Subscripts

- u Upper hemisphere of radome
- l Lower hemisphere

B-4c. Resolution of Forces: To compare theory and experiment it is necessary to resolve force components. The theory of Ref. 1 calculates N_0 and N_θ , whereas the experiment measured integrated values of N_0 and S . The relationship between these components is shown in Fig. 2 below:

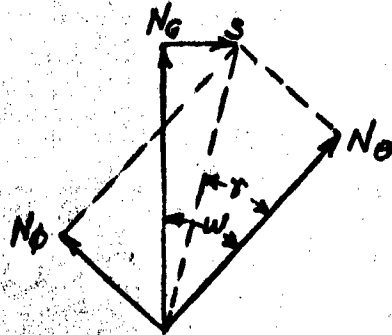


Fig. 2 Resolution of Forces

B-4c(1) Calculation of w : w is the intersection angle between the great circle through the crown and the latitudinal circle normal to the wind direction. The angle between the two circles (or their tangents) varies with azimuth.

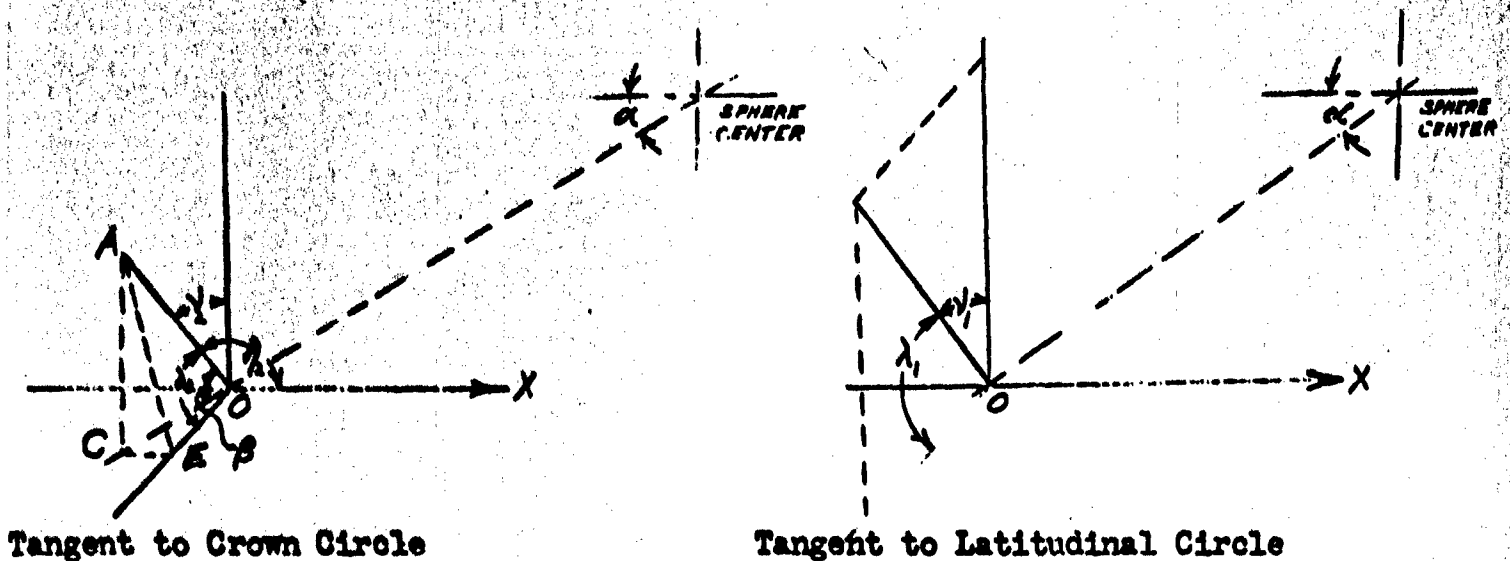


Fig. 3 Tangent Diagrams

Fig. 3 shows diagrams of the two tangents separately to improve clarity. We have the following expression (c.f. Ref. 3):

$$\cos w = l_1 l_2 + m_1 m_2 + n_1 n_2$$

where l , m and n are direction cosines of the two tangents and the subscripts apply to the two different tangents.

For the small circle tangent

$$\lambda_1 = 90^\circ \text{ and } m_1 = \cos \lambda_1 = 0$$

Hence we don't need m_2 or λ_2 .

From the geometry of the figure we have

$$\cos \lambda_2 = \frac{EO}{AO} = \frac{OC \sin \alpha}{AO} = \frac{AO \cos \beta \sin \alpha}{AO}$$

$$l_2 = \cos \beta \sin \alpha$$

$$\nu_2 = 90 - \beta; \quad n_2 = \cos (90 - \beta)$$

$$\lambda_1 = 90 - \nu_1; \quad l_1 = \cos (90 - \nu_1)$$

$$n_1 = \cos \nu_1$$

Hence

$$\cos \omega = \cos (90 - \nu_1) \cos \beta \sin \alpha + \cos \nu_1 \cos (90 - \beta)$$

$$= \sin \nu_1 \cos \beta \sin \alpha + \cos \nu_1 \sin \beta$$

$$\text{But } \nu_1 \text{ is a constant} = \tan^{-1} \frac{h}{A \sin \alpha} = \tan^{-1} \frac{.408}{\sin \alpha}$$

$$\beta \text{ is a constant} = 67^\circ 40'$$

$$\sin \beta = .925, \quad \cos \beta = .380$$

Finally then

$$\cos \omega = 0.380 \sin \left[\tan^{-1} \frac{.408}{\sin \alpha} \right] \sin \theta + .925 \cos \nu_1$$

B-4d. Calculation of Lift from Pressure Distribution

B-4d(1). Theoretical Lift Distribution: The pressure distribution over a classical sphere in viscous flow was assumed as shown in Fig. 4, which was taken from Ref. 1. This distribution was assumed to be symmetric about the wind axis. For a complete sphere no vertical force would exist, but for the truncated radome sphere a vertical force is obtained. This lift

can be expressed in differential form by the equation

$$\begin{aligned} \frac{dL}{q} &= 2Kb \, dx \\ &= 2K\sqrt{B^2 - x^2} \, dx \end{aligned}$$

where L is lift

K is local pressure coefficient

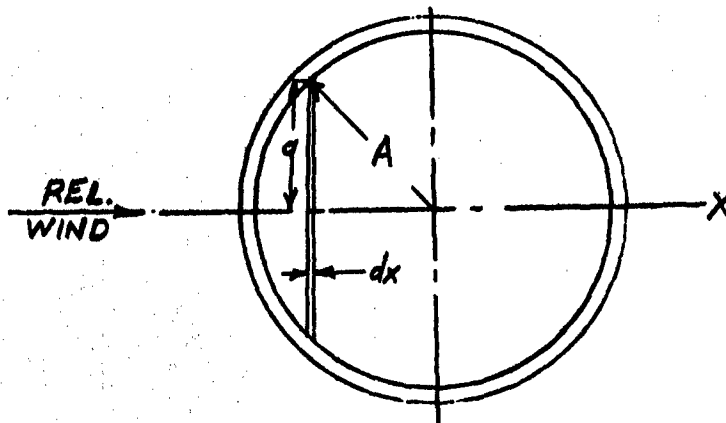


Fig. 5 Lift Elements

The total lift is the integral of the lift over each strip.

$$\frac{L}{q} = 2 \int_{-B}^B K\sqrt{B^2 - x^2} \, dx$$

For the upstream part of the sphere the pressure coefficient could be expressed by the equation

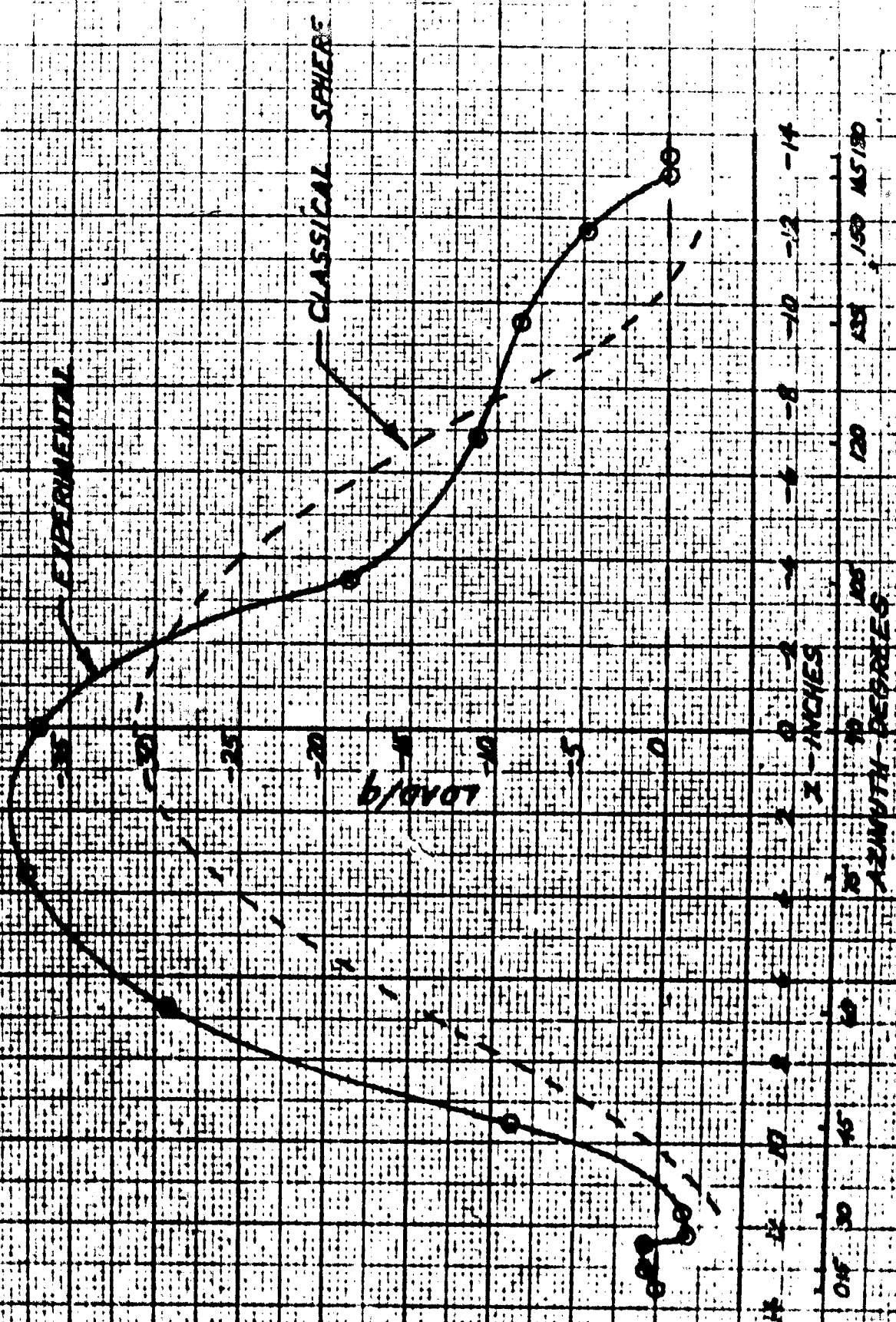
$$K = 1 - \frac{2}{4} \sin^2 \phi \quad (\text{Ref. 4})$$

Because of viscosity, however, the pressure over the downstream part of the sphere does not follow this law. To calculate the total lift then, the expression for dL/q was plotted as in Fig. 6, and a planimeter used to obtain the integrated value of the lift coefficient.

B-4d(2). Lift Calculation Based on Measured Pressure: The calculation of lift from measured pressure is similar in principle to that of the theoretical calculated heretofore. However, the measured pressure over

FIG. 6

MODEL RADON
AFT DISTRIBUTION
AS CALCULATED FROM
PRESSURE DISTRIBUTION
150 MPH 1 ATM



ARMUTHY-DEPTHS

X - INCHES

LOAD/g

EXPERIMENTAL

CLASSICAL SPHERE

the upper hemisphere of the radome was different from that over the lower hemisphere. Therefore, it was necessary to calculate the lift contribution of the upper and lower parts of the sphere separately. For the upper hemisphere we have

$$\frac{dL_u}{q} A = 2 K_u r dx = 2K_u \sqrt{R^2 - x^2} dx$$

For the lower part we have

$$dL_l A = 2 K_l (r - b) dx = 2K_l (\sqrt{R^2 - x^2} - \sqrt{B^2 - x^2}) dx$$

where

$$|x| < |B|.$$

For $|x| > |B|$

$$\frac{dL_l}{q} = 2K_l \sqrt{R^2 - x^2} dx$$

Then the total lift

$$\begin{aligned} \frac{L}{q} = & 2 \int_{-B}^B [K_u \sqrt{R^2 - x^2} - K_l (\sqrt{R^2 - x^2} - \sqrt{B^2 - x^2})] dx \\ & + 2 \int_{-x}^{-B} (K_u - K_l) \sqrt{R^2 - x^2} dx + 2 \int_B^x (K_u - K_l) \sqrt{R^2 - x^2} dx \end{aligned}$$

This expression is also plotted in Fig. 6

B-4e. Calculation of Drag from Pressure Distribution

B-4e(1) Experimental Drag: The hemisphere can be divided into elements normal to flow direction (Fig. 7).

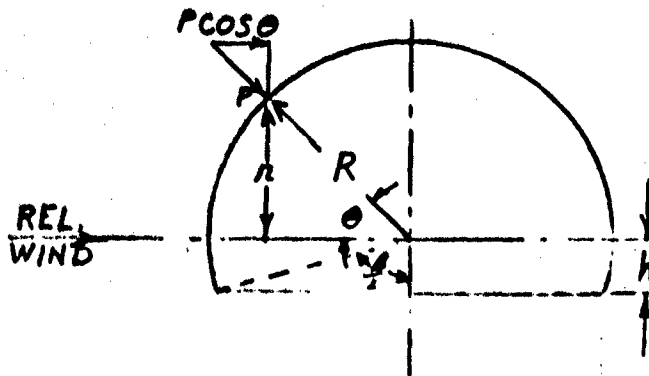


Fig. 7 Radome Side Elevation

Each element has a total area

$$A = \pi r R d\theta = \pi R^2 \sin \theta d\theta$$

The drag force on each element of the upper hemisphere can be expressed

$$d(D_u) = q K_u \pi R^2 \sin \theta \cos \theta d\theta$$

and the total drag is then

$$\frac{D_u}{q} = \pi R^2 \int_0^{\pi} K_u \sin \theta \cos \theta d\theta$$

But

$$R \cos \theta = x ; dx = -R \sin \theta d\theta$$

Therefore

$$D_u = -\pi q \int_{-R}^R K_u x dx$$

On the lower surface the area is a function of x. Each element has a total area

$$A_l = 2r \left(\frac{\pi}{2} - \frac{\beta}{2} \right) R d\theta = 2R^2 \sin \theta \left(\frac{\pi}{2} - \frac{\beta}{2} \right) d\theta$$

Where

$$\frac{\beta}{2} = \tan^{-1} \frac{\sqrt{B^2 - x^2}}{h}$$

$$d(D_l) = q K_l 2R^2 \sin \theta \cos \theta d\theta \left(\frac{\pi}{2} - \frac{\beta}{2} \right)$$

Substituting as above for the functions of θ

$$\frac{D_l}{q} = -2 \int_{-R}^R K_l \left(\frac{\pi}{2} - \frac{\beta}{2} \right) x dx$$

Note that for

$$|x| > |B|, \beta = 0$$

The total drag can then be expressed

$$\frac{D}{q} = \frac{D_u + D_l}{q} = - \int_{-R}^R \left[\pi K_u + 2K_l \left(\frac{\pi}{2} - \frac{\beta}{2} \right) \right] x dx$$

B-4e(2). Theoretical Drag: The theoretical drag can be calculated using the final equation of paragraph B-4e(1) above. In theory however,

$$K_u = K_l = K$$

and the equation simplifies to

$$\frac{D}{q} = - \int_{-R}^R K \left(2\pi - \frac{\theta}{2} \right) x dx$$

B-4f. Envelope stresses: The calculation of envelope stresses is done according to the methods of Ref. 1.

$$P_T = P_\phi + P_\theta = (N_\phi + N_\theta) R$$

where P_T is the total pressure differential across the envelope and P_ϕ and P_θ are components of P_T in the ϕ and θ directions respectively.

B-5. Measurement Procedures

B-5a. Pressures

B-5a(1). General: Sixty eight pressure taps were installed in the radome and tower for sensing local pressure during tests. The taps were fabricated of steel hypodermic tubing installed carefully so as not to project beyond the local surface of radome or tower. Inside the radome the tubes were connected to Cannon connectors by means of flexible plastic tubing. Thus, it was possible to connect and disconnect the pressure lines quickly during model changes. All pressure leads were checked for leaks and blockage; all defects in the system were corrected before the tests. Pressures were recorded by photographing a backlighted manometer board.

B-5a(2). Envelope Pressure: Forty-nine pressure taps were installed in the radome envelope. Each tap consisted of an .065 inch outside diameter tube with an .043 inch inside diameter. The tubing was inserted into a plastic button which was cemented to the inside surface of the radome. The pressure taps were installed on one side of the radome only, but effectively covered the area from top to bottom and front to rear.

B-5a(3). Tower Pressures: Eighteen pressure taps were installed on the tower, three on each of six faces from front to rear. The taps were installed in the center of each face and spaced equally from top to bottom. The tubes were cemented in place in holes drilled in the wood..

B-5a(4). Pressure Inside Envelope: Air was supplied to the envelope from a high pressure line. A continuous supply was required because there was some leakage. Pressure inside the envelope was controlled by a needle valve in the line. A U-tube containing Merriam unity oil (specific gravity of 1) was used to measure the internal pressure. One side of the U-tube was connected to the tunnel stagnation pressure, the other side to the inside of the envelope.

B-5b. Forces

B-5b(1). Force measurements were made during the model tests with strain gages installed on the lift, shear and pedestal beams (Fig. 8). The resulting strain gage signals were recorded by an oscillograph system, com-

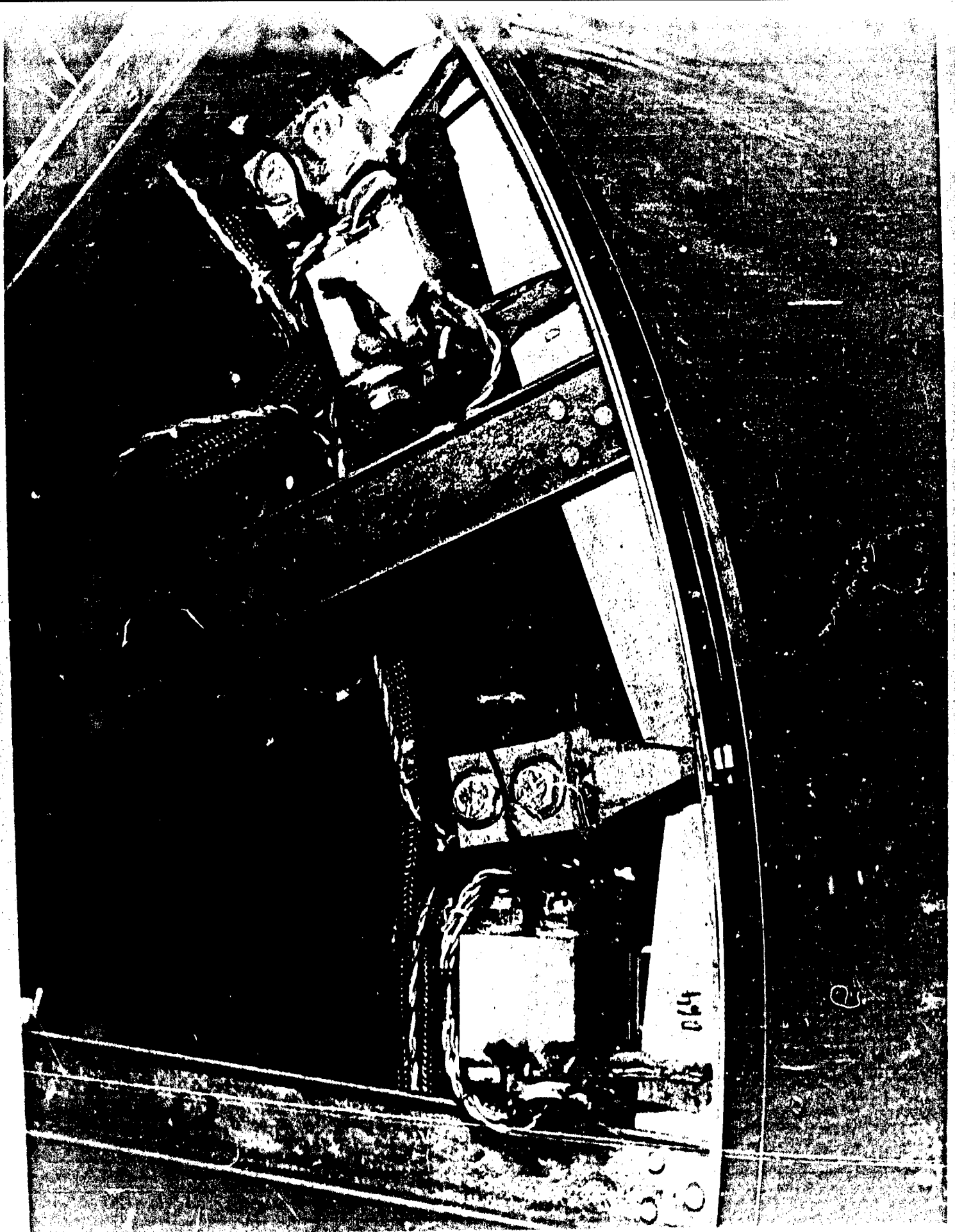
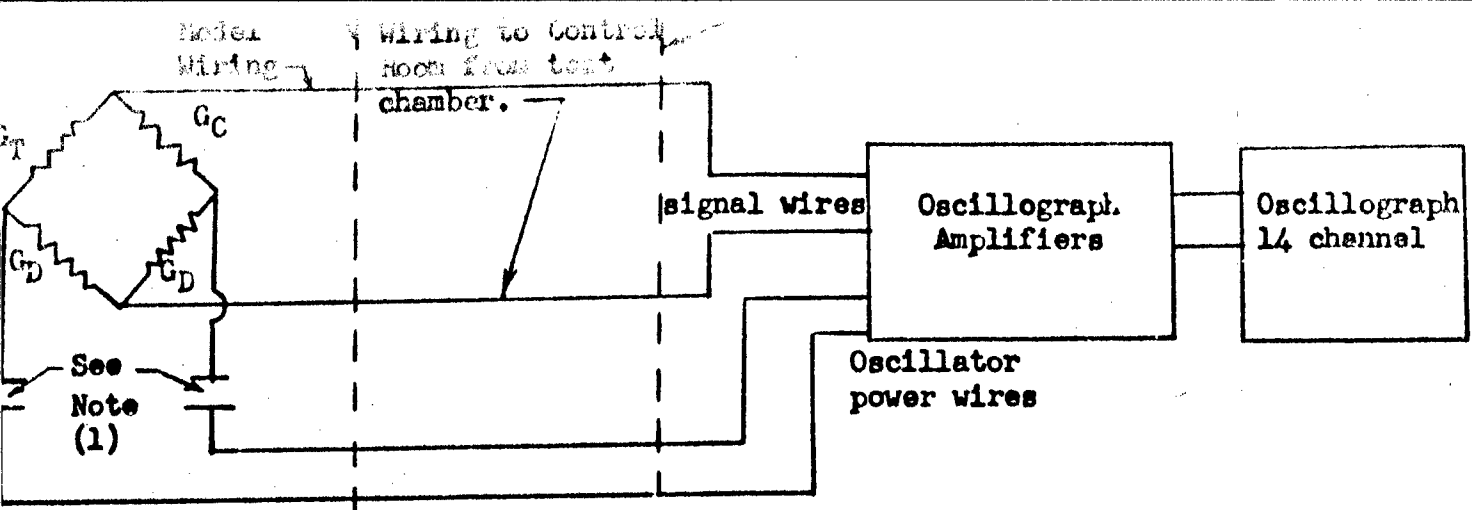
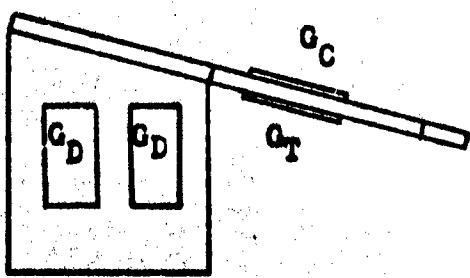


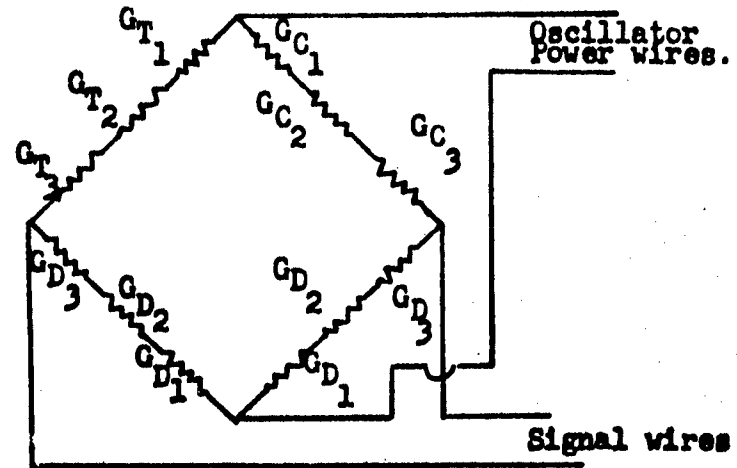
Fig. 8
Lift and Shear Beams



Typical Instrumentation Wiring



Typical Gage Location



Summation Gage Wiring of Pedestal Beams

Notes:

- (1) All strain gage bridges feeding each amplifier unit are powered by the same wires.
- (2) All strain gages bonded to the measuring beams with Duco cement and moisture proofed with Petrosene wax.
- (3) All wiring is shielded from the model to the oscillograph amplifier

- G_C - strain gage in compression (normal loading)
- G_T - strain gage in tension (normal loading)
- G_D - strain gage dummy

SCHEMATIC DIAGRAM OF STRAIN GAGE INSTALLATION

FIGURE 9.

posed of a 14 channel Consolidated Engineering oscillograph and associated amplifiers and galvanometers. This basic system uses a 3KC carrier and has an overall frequency response of 500 cps. Since the measuring equipment was capable of high gain, the measuring beams were designed for operation with low stresses. This was done to limit the amount of relative motion between the tower and the radome and thus minimize the possibility of model flutter. A two-active-arm strain gage bridge was used on each measuring beam in a manner that would produce tension in one gage and compression in the other when the beam was loaded. To prevent temperature effects and "cross talk" the dummy gages were mounted on the beam base to complete the bridge. "Petrosene" was applied over the completed assembly to affix the small wires and provide moisture resistance.

As an additional precaution against "cross-talk" and heterodyning or "beating" of the strain gage signals, the oscillators supplying bridge voltage to the strain gages were synchronized together. In this way, all carrier voltages to and from the bridges were in phase.

B-5b(2). Since it was necessary to support the pedestal plate with three beams for the measurement of pedestal reaction, a summation strain gage circuit was required as shown in Fig. 9.

B-5b(3). The complete recording system was installed and prepared for use before the calibration was made. The model was installed in the test area and a dead weight calibration of each load beam was performed.

C. DETAIL FACTUAL DATA

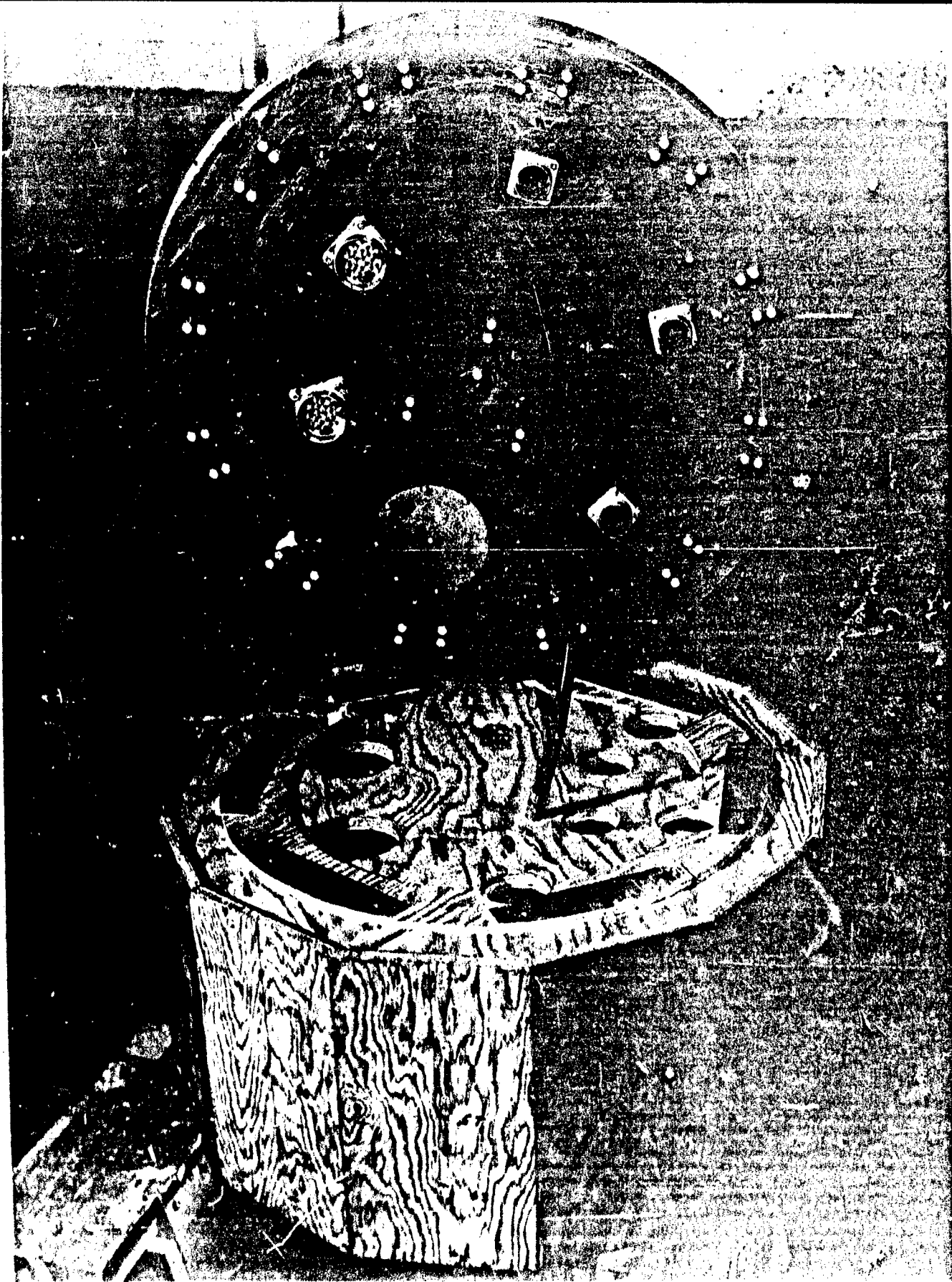
C-1. Model

C-1a. Envelope

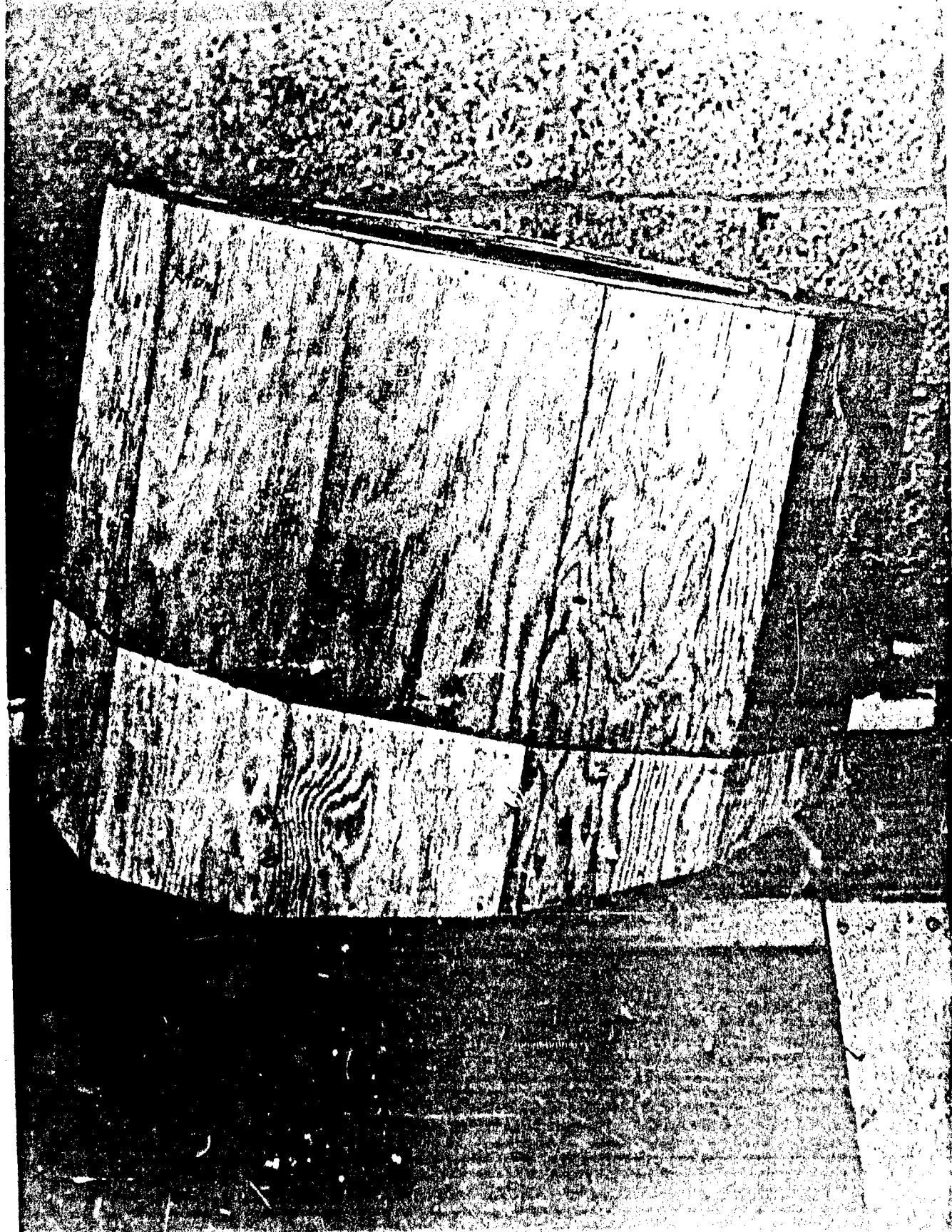
C-1a(1). The envelope was fabricated from a two-ply, 45° bias constructed, neoprene coated nylon ballonet material, weighing a total of 6.60 ounces per square yard. It was obtained through the Airship Development Department of the Goodyear Tire and Rubber Company, Akron, Ohio.

C-1a(2). The envelope was fabricated of 24 gores, plus a five-inch diameter crown. A flat template was made for the gores, the template being calculated to provide a sector of a 27-inch diameter sphere with a cut-off at a base angle of 67° 40'. An overlap of 1/2 inch was allowed on each joint. The gores were arranged with alternate right and left bias to avoid possible twist due to uneven tension in the plies. Goodyear type 1822-C Neoprene cement with Type 983 Accelerator was used to cement the fabric.

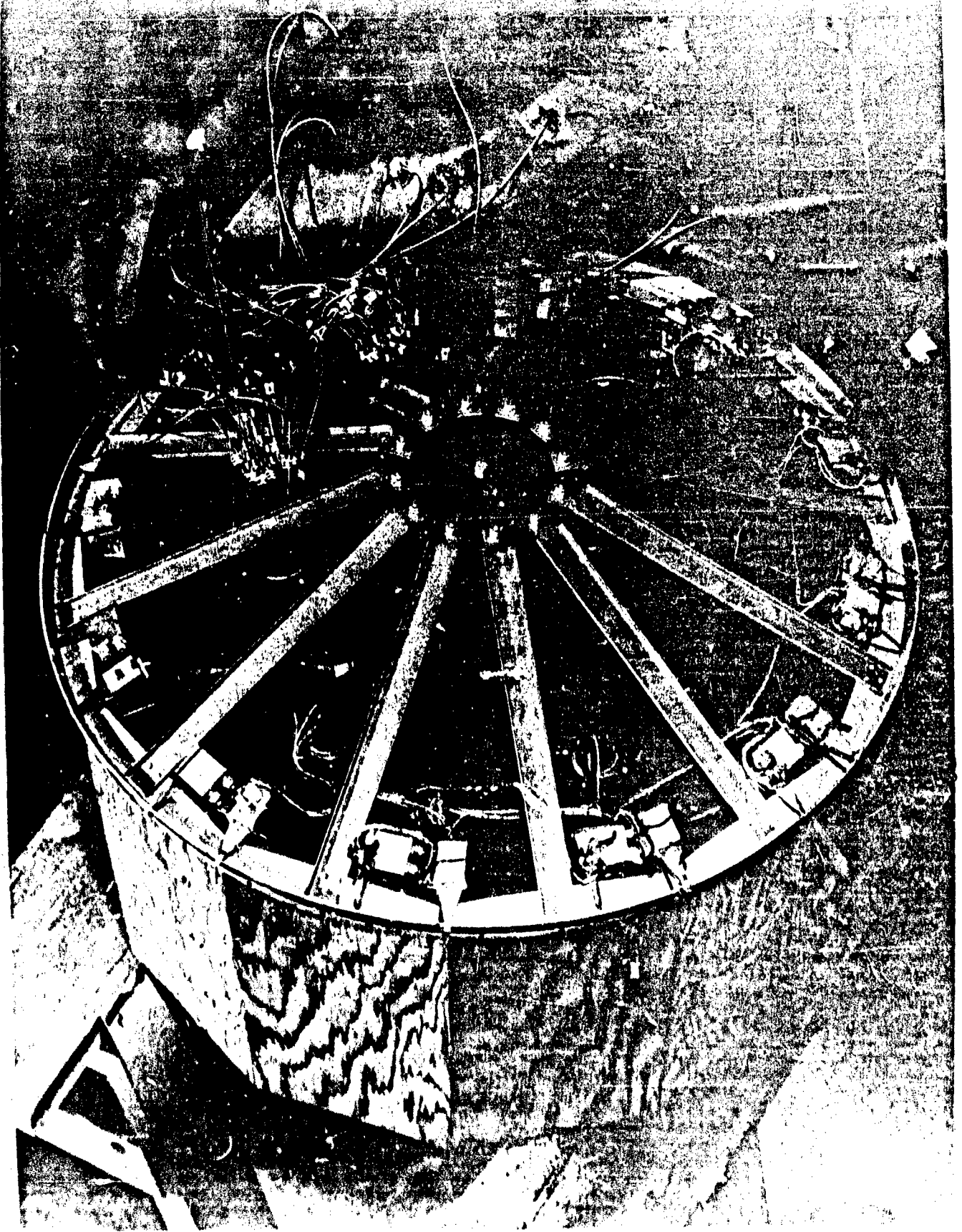
C-1b. Construction of Tower (See Figs. 10 and 11): The tower was 12 inches high and 12-sided to simulate the AN/FPS-6 arctic tower. The model tower was 25 inches across the vertices. It was constructed of 1/2 and 3/4 inch fir plywood, gusseted for rigidity. Two wedges were similarly constructed to provide for tilting the tower 15 and 30 degrees to simulate the effect of a hilltop installation (Fig. 11). Attachment of the tower to the wedges and to the tunnel floor was made by bolts. The bottom of the tower had a large hole to permit access to instrument attachments.



MODEL TOWER
Fig. 10



MODEL TOWER & WEDGE
FIG. 11



BALANCE SYSTEM
Fig. 12

C-1c. Balance System: The balance system is shown in Fig. 12. The system was designed to indicate lift and shear forces at 12 evenly spaced positions around the radome, thus simulating the load distribution into the 12 columns of the full-scale tower. Actually, forces were measured on only one side of the radome because of physical and aerodynamic symmetry. Nevertheless, the dummy beams and supports were identical to those in the "live" side except for the lack of strain gages. The entire system was mounted on a 1/4 inch steel plate containing necessary openings for instrumentation leads.

The forces from the envelope were introduced into the measuring beams through a 12-sector ring at the base of the radome. The shear load on each 30-degree sector was measured by one beam. The lift beams were located at the ends of the sectors so that each lift gage measured part of the load from each of the two sectors. Each lift beam was oriented to measure loads tangent to the surface of the radome. Although the force and reaction were applied as close to the surface as possible, a small couple actually existed. The effect of this couple was to increase the measured lift. Since the error was slight and in the conservative direction, no correction for it has been made in this report.

Each sector of the base ring was connected by a metal channel to a circular plate at the center of the radome. The plate was supported by a shaft but could move laterally so as to indicate horizontal forces on three beams. These beams measured that part of the drag resulting from envelope distortion which was not measured by the shear gages. The lift was measured by seven beams and the shear by six others. The circuitry and instrumentation associated with this system are described in para. B-5b.

C-1d. Pressure Taps: The pressure taps are described in paragraph B-5a.

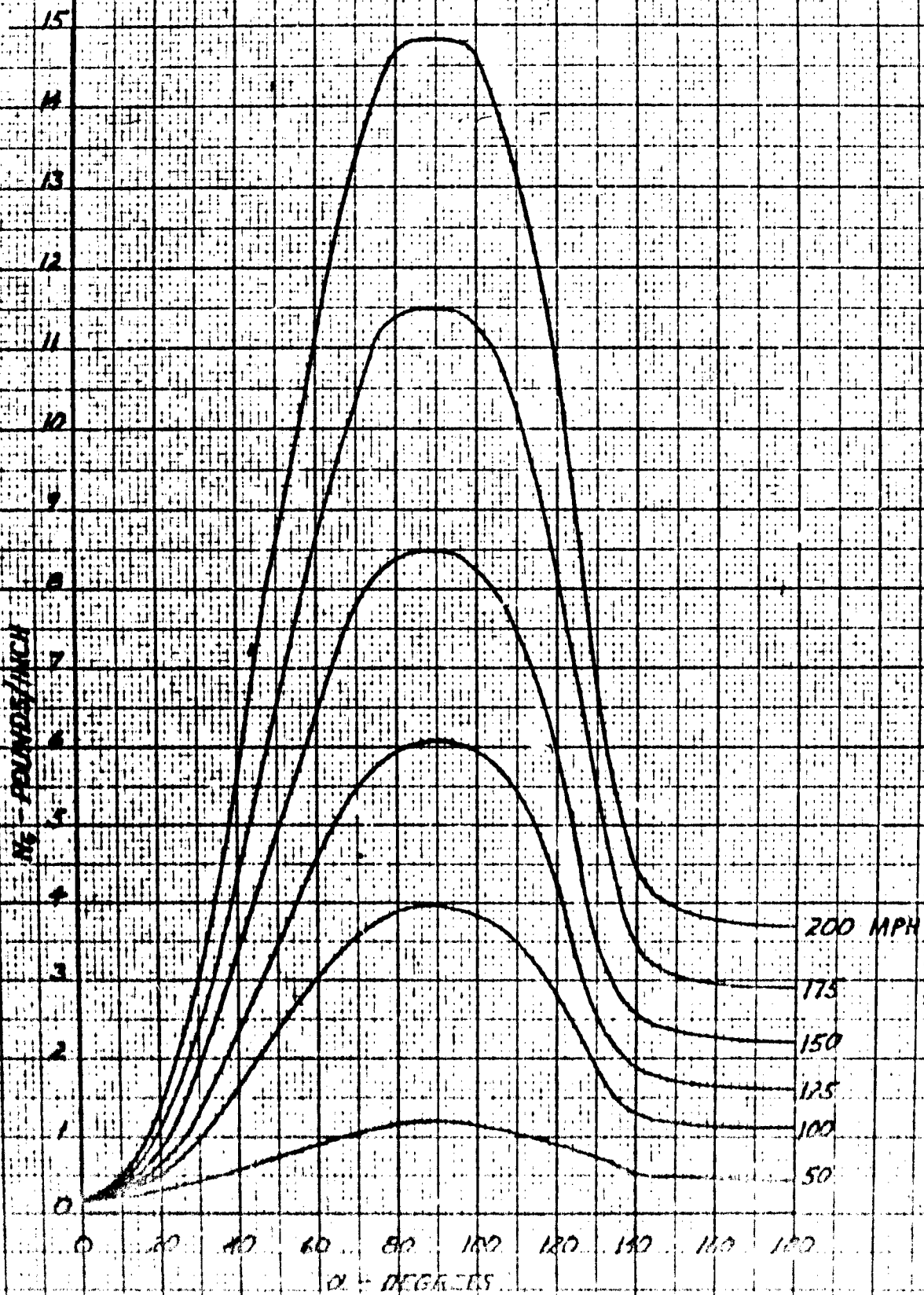
C-2. Data - Comparison of Measured and Theoretical

C-2a. General: For design purposes there are a number of loads which must be determined. These are:

1. Lift distribution
2. Over-all lift
3. Shear distribution
4. Over-all drag
5. Envelope stresses

There are several possible ways of arriving at these values for the model, including both experimental as well as theoretical considerations. The two experimental methods serve as a check on the accuracy of the test data since they are directly comparable. In the following paragraphs a discussion of these methods will be given along with a chart comparison of the various results. It will be noted that the experimental data give generally higher loads than the theoretical calculations. As explained in paragraph C-6, the increase is due to the difference between the actual and assumed pressure distributions which are shown in Fig. 4.

FIG. 10
MODEL RADOME
CALCULATED LIFT LOADS
1 ATM.



T A B L E I

Comparison of Measured and Theoretical Data

Loading	Lift Distribution	Over-all Lift (lbs.)	Maximum Shear (lbs./in.)	Over-all Drag (lbs.)	Maximum Envelope Stresses (lbs./in.)
Experimental, based on balance system	Fig. 11	180	0.9	51.2* 39.8	-
Experimental, based on pressure measurements	Fig. 6	186	-	52.1* 40.5	9.00
Based on classical sphere pressure dist.	Fig. 6	142	-	30	8.48
Based on Radome Manual	-	128.5	1.4* 1.2	54.2* 46.8	8.48

* Extrapolated values based on full scale Reynolds' number (See para. C-4).

C-2b. Lift Distribution

C-2b(1). The balance system measured forces imposed by 30-degree sectors corresponding to column spacing in the AN/FPS-6 tower. These forces thus represent a column loading imposed by the radome envelope loads. In order to compare the measured forces with theory, the theoretical load distribution, based on the data of Ref. 1, was calculated. This method provides the magnitudes of forces along latitudes and longitudes of the sphere, whereas the forces measured by the model balance were those along great circles passing through the crown (top of vertical center line of the radome). As indicated in paragraph B, it was necessary, therefore, to resolve N_{θ} and N_{ϕ} into the direction of N_{θ} and S. The equations and methods of calculation are discussed in paragraph B-4c of this report.

C-2b(2). Fig. 13 is a plot of theoretical N_{θ} as a function of the azimuth angle θ . In order to obtain the theoretical loading of the strain gages the over-all contribution of the various sectors was determined by graphical integration using a planimeter. The planimeter was also used to determine the centroid of the load areas. The load on each lift gage then consisted of contributions from the two sectors on each side of it. Each sector load was apportioned according to the centroid of its load area.

FIG. 14-0
 MODEL RADOME
 BASE LIFT LOADS
 1 ATM.

KEY
 THEORETICAL CURVE —
 EXPERIMENTAL POINTS
 GAGE #1 (0°) - - - - - ○
 2 (30°) - - - - - △
 3 (60°) - - - - - ⊙
 4 (90°) - - - - - □

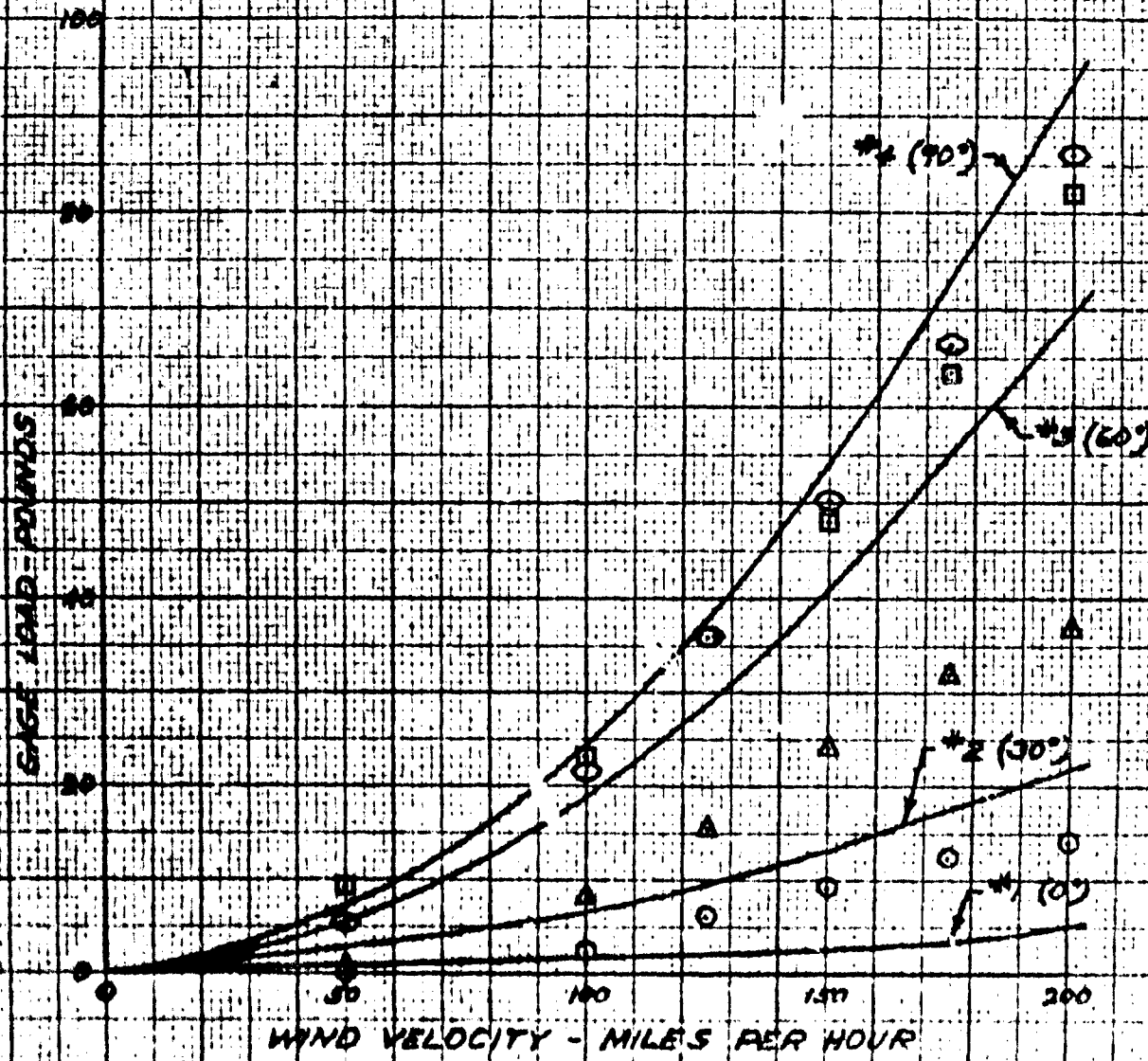
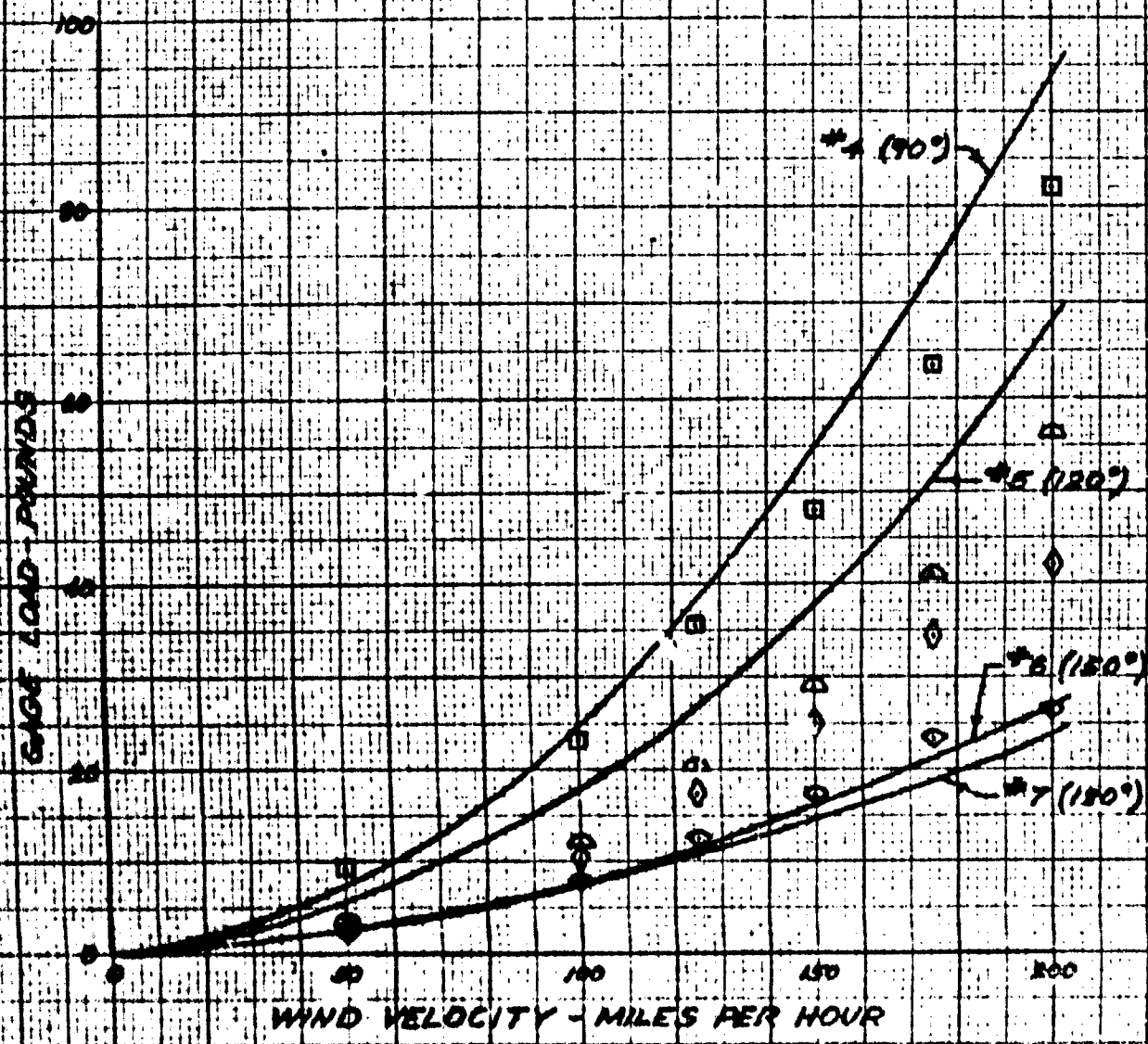


FIG. 14 B
 MODEL RADOME
 BASE LIFT LOADS
 1 ATM

KEY
 THEORETICAL CURVE ———
 EXPERIMENTAL POINTS
 GAGE #4 (90°) - - - - - □
 5 (120°) - - - - - △
 6 (150°) - - - - - ◇
 7 (180°) - - - - - ○



C-2b(3). Comparison of the theory with the actual strain gage loading is shown in Figs. 14a and 14b. It can be seen that the measured loads are higher than the calculated at all points except for the gages at $\theta = 90$ and 120 degrees. This agrees closely with the pressure distribution of Fig. 4 which shows higher negative pressures at all points except in the region from about 90 to 120 degrees.

C-2c. Over-all Lift

C-2c(1). Experimental: The over-all lift on the model can be determined by two methods. One involves summing up the contributions from all lift gages, taking into account the fact that the gages were installed along only one side of the model. After subtracting the upward force due to internal pressure in the radome, the actual aerodynamic lift can be obtained. At 150 miles per hour and a tunnel pressure of one atmosphere, the aerodynamic lift thus calculated was 180 pounds. The second method of calculating over-all lift is to integrate the pressure distribution over the radome. The method used is outlined in paragraph B of this report. The total lift thus calculated for the 150 mile per hour condition was 186 pounds. Although this figure is a little higher than that obtained by strain gage measurement, the difference is within the experimental error.

C-2c(2). Calculated Lift: The lift can be calculated by two different methods. One of these involves integrating the classical pressure distribution over the radome as described in paragraph B-4d. of this report. Assuming a truncated sphere in a viscous fluid, the total lift obtained by this method was 142 pounds. The second method of calculation is given in the Radome Design Manual, Ref. 1. We have the following data for the model:

$$\begin{aligned} R &= 13.5 \text{ inches} \\ U &= 150 \text{ mph} \\ q &= .3674 \text{ psi} \\ p_0 &= .3674 + .036 = .4034 \text{ psi} \end{aligned}$$

Following the procedure in Appendix I of Ref. 1 :

$K_p = 1.92$ and the over-all lift = $1.92 \times .3674 \times 13.5^2 = 128.5$ pounds. This value varies from the purely theoretical case because it takes into account a correction factor for the effect of aerodynamic interaction between the envelope and tower. The reason for both of the calculated figures being lower than the experimental is explained in paragraph C-6.

C-2d. Shear

C-2d(1). Experimental Shear: Shear forces were measured at the base of the radome by strain gages mounted on beams arranged to bond in the fore and aft directions (See Fig. 8). Each beam was actuated by the sum of forces on a 30 degree sector. The results of these measurements are shown for the one atmosphere condition in Fig. 15. Since the experimental points in Fig. 15 represent integrated values of shear loading, the maximum unit shear is not known accurately. A sinusoidal distribution is indi-

FIG. 15
 MODEL RADOME
 BASE SHEAR LOADS
 1 ATM

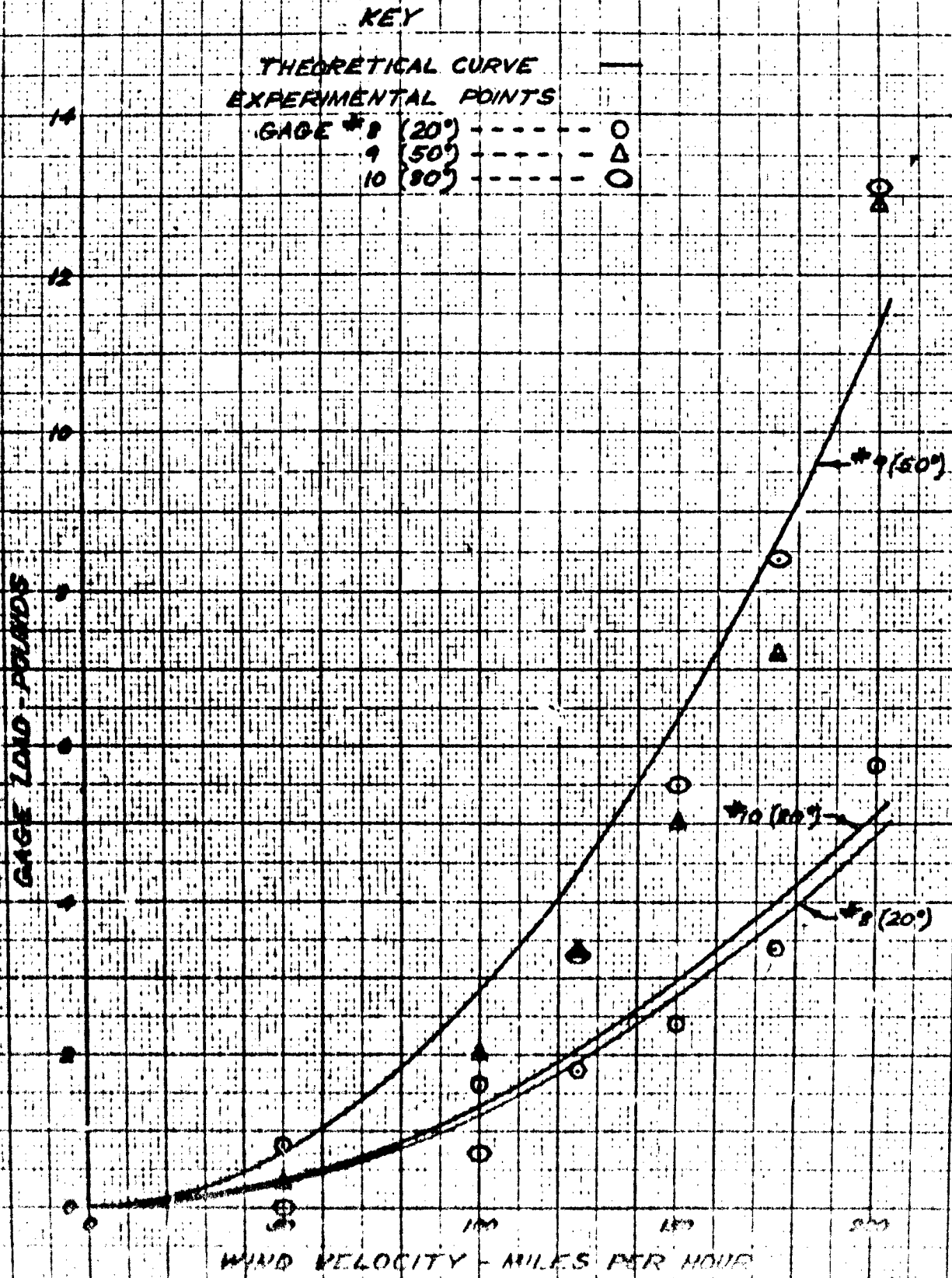
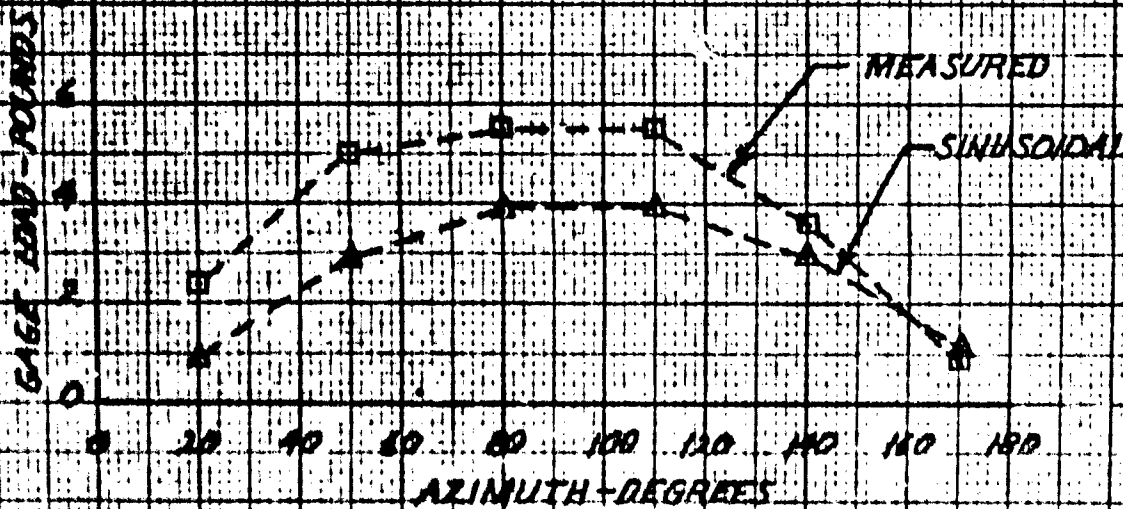


FIG 16
MODEL RADOME
BASE SHEAR DISTRIBUTION
150 MPH 1 ATM.



cated however, since the general distribution of the loading is quite similar to that of a sinusoidal distribution as can be seen in Fig. 16. In the region of maximum shear the distribution appears fairly flat. Therefore, it would be reasonable to calculate the approximate maximum shear load simply by dividing the faired value in Fig. 16 by the length of arc. This gives a maximum shear value of approximately 0.9 pounds per inch.

C-2d(2) Calculated Shear: The shear can be calculated from the resolution of the forces N_{ϕ} and N_{θ} as described in paragraph B-4c. However, this calculation does not account for the redistribution of load in the fabric and base so that a misleading indication of the true shear is obtained by this method. The Radome Design Manual (Ref. 1) recommends the use of a sinusoidal shear distribution which seems to indicate reasonably well the general shape of the measured shear distribution. Comparisons between the measured and calculated shear loadings is given in Fig. 16. The maximum unit shear load predicted by this method can be calculated from the equation (according to Appendix I, Ref. 1).

$$S = 3.18 K_D q R / \sin \beta$$

where K_D is the corrected drag coefficient
 β is the base angle

In the 150 miles per hour test we obtained

$$S = .318 \times .7 \times .3674 \times 13.5 / .925 = 1.2 \text{ pounds per inch}$$

If the extrapolated drag coefficient (Fig. 19) is used

$$S = 1.4 \text{ pounds per inch}$$

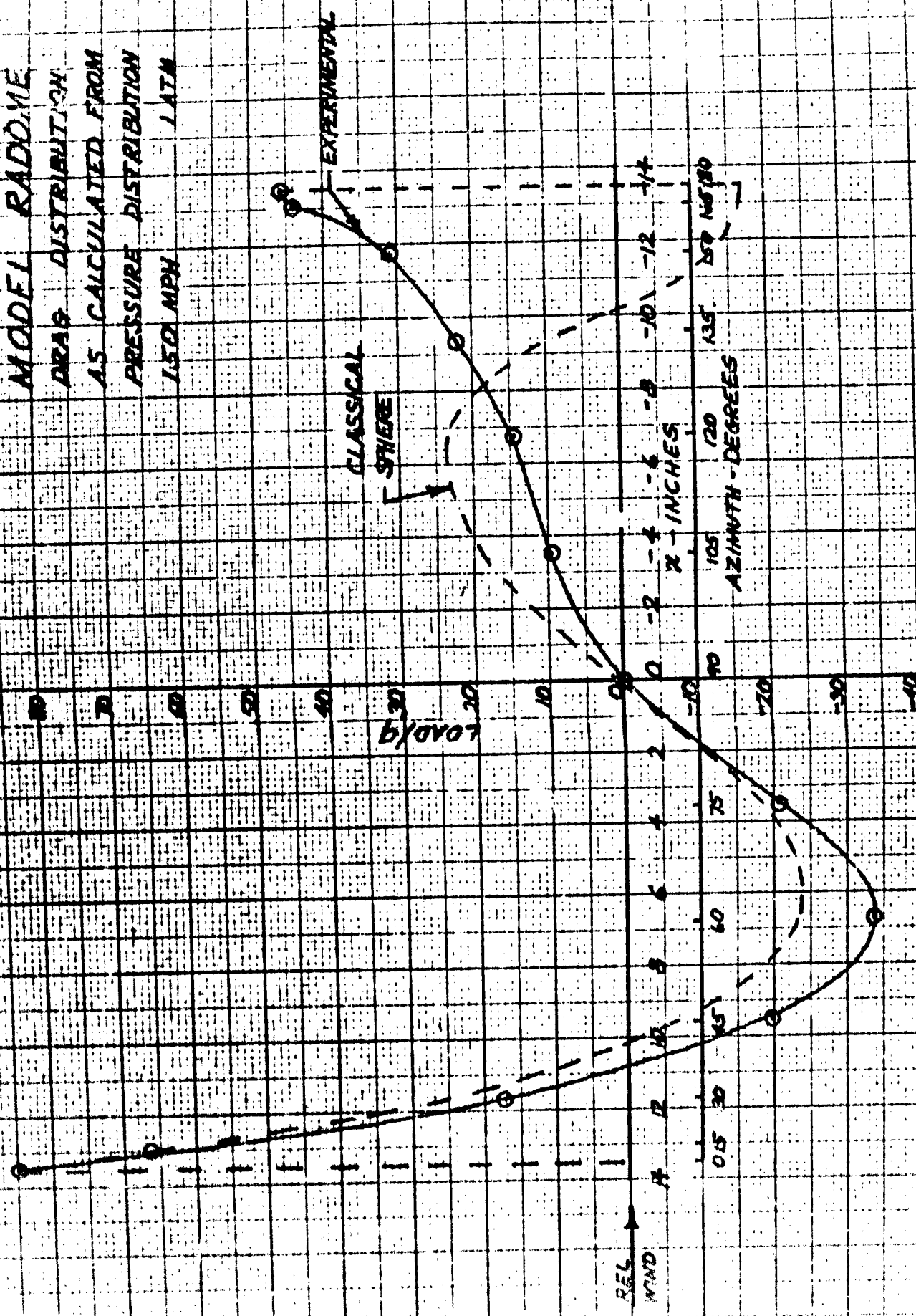
C-2e. Over-all Drag

C-2e(1). Experimental: Two methods exist for calculating the total drag from the wind tunnel test data. One method is to sum up all the rearward components of the shear gage loads taking into account the fact that the gages were mounted on only one side of the radome. If the force measured by a strain gage is called F, then the contribution of the gage to drag is $F \sin \alpha$. The total of all the rearward forces thus summed for the 150 miles per hour, one atmosphere test, gives a total drag of 39.8 pounds. The second method of calculating the drag is to sum up the rearward components of the pressure forces. This method of calculation is detailed in paragraph B-4e. Fig. 17 is a graph of the drag forces as a function of fore and aft location. Integration of these forces by means of a planimeter results in a drag of 40.5 pounds from the experimental pressure distribution which agrees closely with the strain gage result.

C-2e(2). Theoretical: The theoretical drag can be calculated by integrating the forces resulting from the classical pressure distribution as detailed in paragraph B-4e. The result of this calculation is a total drag of 30 pounds at 150 miles per hour. This figure is lower than the ex-

FIG. 17

MODEL RADO.ME
DRAG DISTRIBUTION
AS CALCULATED FROM
PRESSURE DISTRIBUTION
150 MPH 1.1A



perimental drag because the assumed pressure distribution is lower, as is discussed in paragraph C-6. Another calculation is recommended in the Design Manual (Ref. 1). We have the equation

$$D = K_D q R^2$$

where K_D is the drag coefficient. Appendix I of Ref. 1 recommends a value of $K_D = .7$ which takes into account the interference between the tower and the envelope. Calculating for the 150 miles per hour test

$$D = .7 \times .3674 \times 13.5^2 = 46.8 \text{ pounds}$$

This result is somewhat higher than the experimental drag. However, the tests show that the effect of increasing Reynolds' number is to increase the drag coefficient (See para. C-4). If this increase is taken into account a drag coefficient of about 0.81 is indicated. Then

$$D = 0.81 \times .3674 \times 13.5^2 = 54.2 \text{ pounds}$$

C-2f. Envelope Stresses

C-2f(1) Experimental: In accordance with Ref. 1, the envelope stresses are divided into two perpendicular components, N_ϕ and N_θ , which can be considered as acting along lines analogous to latitudes and longitudes on the earth. On the radome the longitudes all pass through the stagnation point which thus is analogous to the North Pole. N_ϕ represents the force per unit length along a longitudinal line while N_θ represents the latitudinal force. The region of maximum fabric loading occurs somewhere in the region between the maximum diameter and the point where the net drag force is zero (approximately $\alpha = 60$ degrees). The calculation is made by considering that N_ϕ at any point must balance the sum of all drag components plus the internal pressure to that point. The sum of the drag components is determined by integrating the area under the drag distribution curve, Fig. 17, from the stagnation point to the point under consideration. In these calculations, redistribution of drag load through the envelope to the base is neglected. This results in a slightly conservative value for N_θ . In determining values for design, the calculated value of N_ϕ (at the base) is corrected to include a term based on drag distribution (Ref. 1, Appendix I).

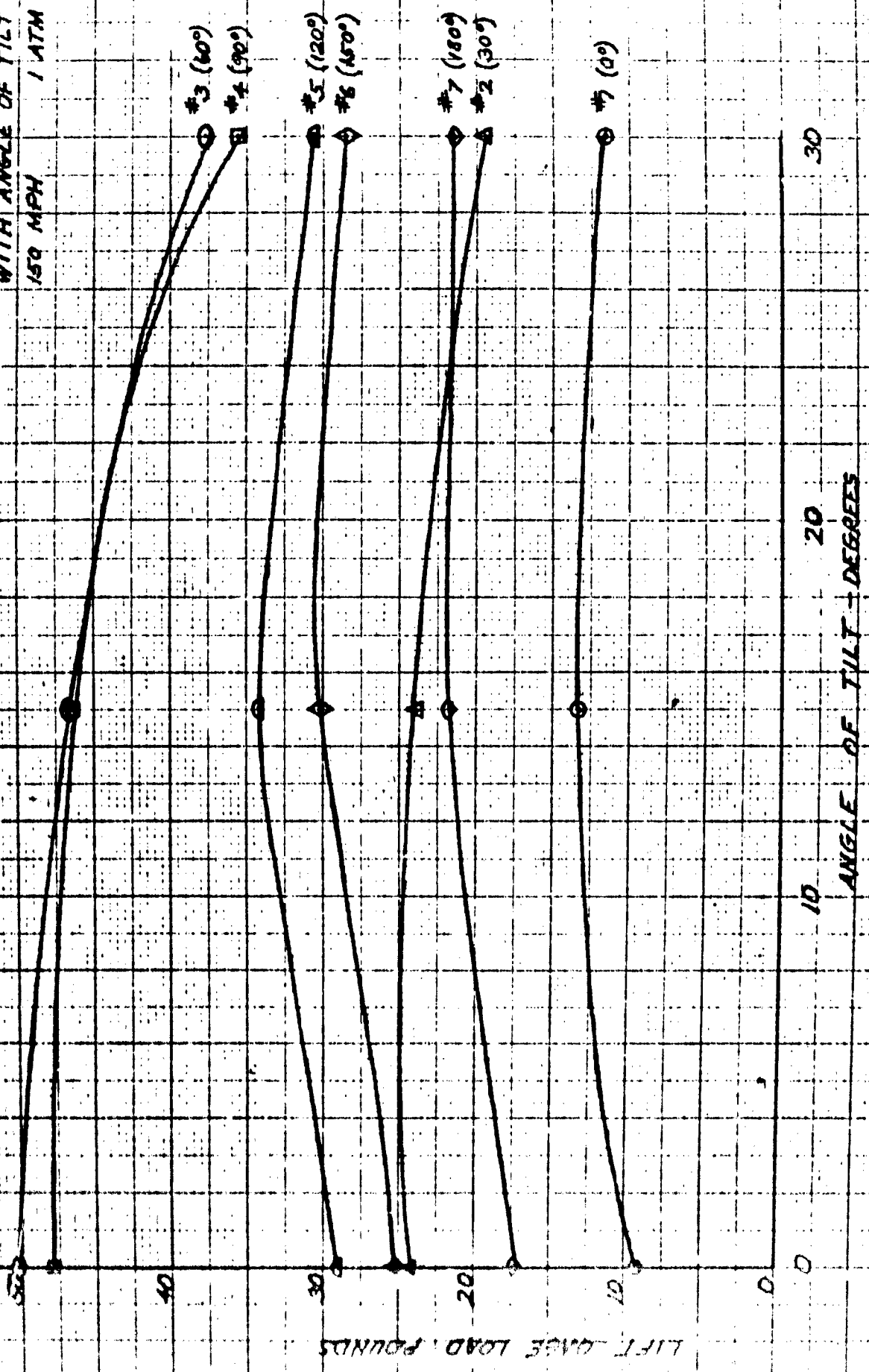
The following are the equations used:

$$N_\phi = \frac{L_i + L_D}{2 \pi r}$$

where L_i is the fabric load due to internal pressure and L_D is the load due to drag.

$$N_\theta = r \Gamma_\theta = r(P_T - P_\phi) = r\left(P - \frac{N_\phi}{R}\right)$$

FIG. 18
MODEL RADOME
VARIATION OF LIFT
WITH ANGLE OF TILT
150 MPH
1 ATM



P_T is the total pressure difference across the radome surface at the point in question as determined by subtracting the external from the internal pressure. The following table is a summary of the results for several points in the region in question:

α	N_{ϕ}^*	N_{θ}
60.7	2.91	8.03
75	3.85	9.00
90	4.04	8.51

* Uncorrected for redistribution of drag.

It is apparent that the maximum fabric load occurs at about the 75 degree position.

C-2f(2) Calculated: The maximum envelope stress can be calculated by using the formula given in Appendix I of Ref. 1. The stress at the base is given by

$$\begin{aligned} N_{\theta} &= (1.16q + .5P_0)R \\ &= (1.16 \times .3674 + .2017)13.5 \\ &= 8.48 \text{ pounds/inch} \end{aligned}$$

$$\begin{aligned} N_{\phi} &= (.193q + .5P_0)R + .635 K_D qR \\ &= (.193 \times .3674 + .2017)13.5 + .685 \times .7 \times .3674 \times 13.5 \\ &= 5.88 \text{ pounds/inch} \end{aligned}$$

It can be seen that the maximum fabric stress as calculated from the experimental data is slightly higher than the calculated.

C-3. Effect of Terrain: A likely choice for a radome installation site would be a hilltop. In order to investigate the effect of such terrain on the radome aerodynamic forces, two wedges were fabricated. These wedges, which were 12-sided like the tower, tilted the tower back 15 and 30 degrees respectively to simulate the effect of winds sweeping up a hill. The results of these tests on the lift gages are shown in Fig. 18. It can be seen that no substantial change in loading occurs with angle of tilt. The maximum loads as shown by the gages at 60 and 90 degrees show a reduction of load as the tower is tilted.

C-4. Effect of Reynolds' Number: Reynolds' number is known to affect the point of boundary layer transition. At very low Reynolds' numbers the boundary layer is laminar and separation of flow occurs close to the maximum sphere diameter. However, when the Reynolds' number is above "critical",

FIG. 17

MODEL BALLS
EFFECT OF REYNOLDS' NO.

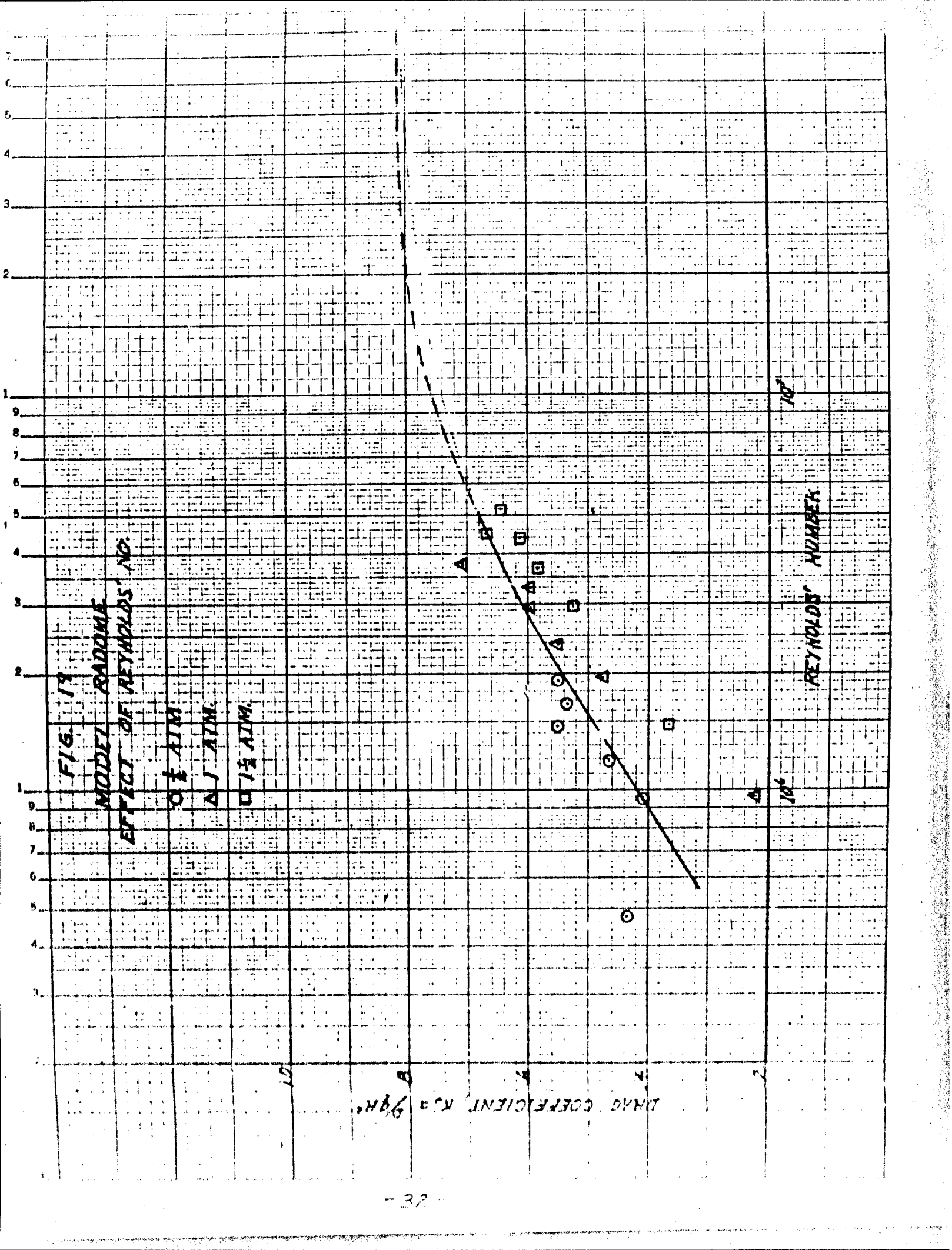
○ 1/4" AIR

△ 1/2" AIR

□ 1 1/2" AIR

DRAO COEFFICIENT $C_D = \frac{D}{\rho V^2 A}$

REYNOLDS' NUMBER



the boundary layer is turbulent and separation is delayed until the flow is well back along the sphere. Thus the wake and, therefore, the drag is reduced. For a sphere, the critical Reynolds' number is in the range of about 220,000 to 280,000, (Ref. 2). The Reynolds' numbers of the tests reported herein ranged from about 500,000 to 5,000,000, which is well above the critical, although below the full scale value of over 100,000,000.

Early test results with the radome had indicated an upward trend in drag coefficient with Reynolds' number above critical. Therefore, higher drag values than those measured were recommended in Ref. 1. In order to obtain further information on this point, the more recent wind tunnel tests were run at the widest possible range of Reynolds' numbers. In Fig. 19, the measured drag coefficient for the various wind tunnel tests with the tower level are plotted as a function of Reynolds' number. A definite upward trend appears in the data. A curve drawn through the data is extrapolated to about the full scale radome Reynolds' number. The shape of this curve was chosen to be roughly similar to the usual asymptotic shapes found in such curves. See, for example, Ref. 2. Unfortunately, there are no other data for such large Reynolds' numbers so that the accuracy of the extrapolation cannot be checked. In view of the scatter of the data, high accuracy is not claimed for this curve, but the maximum value is believed to be conservative. No large change in pressure distribution would be expected to occur at such a high range of Reynolds' numbers because the effect of viscous forces would be vanishingly small.

C-5. Effect of Internal Pressure: During the wind tunnel tests the internal pressure of the radome was usually kept at one inch of water pressure above stagnation pressure. In some of the tests, however, the internal pressure was varied over a range of plus or minus two inches of water from the stagnation pressure. No change in radome behavior was noted except for some flattening of the envelope in the stagnation region. Examination of the pressure data indicated a small change in pressure distribution, particularly at the lowest internal pressure. The change was small, however, so that the tolerance for internal pressure can be increased.

C-6. Wind Tunnel Blockage Correction: Because the maximum Mach number of the test was fairly low and the tunnel large compared to the model, wind tunnel blockage corrections were expected to be small. The correction will be calculated here by the method of Ref. 5, to show that such is the case.

The corrections to Mach number and dynamic pressures are as follows:

$$M = M_u \left[1 - C(1 + 0.2 M_u^2) \right]$$
$$q = q_u \left[1 + C(2 - M_u^2) \right]$$

where

M_u is uncorrected Mach number

q_u is uncorrected dynamic pressure

C is blockage correction factor

$$C = C_w + C_b + C_{wk}$$

$$C_w \text{ is the wing (tower) blockage correction} = \frac{1}{\beta^3} \frac{K_1 T_w V_w}{C^{3/2}}$$

$$C_b \text{ is the body (sphere) blockage correction} = \frac{1}{\beta^3} \frac{K_2 T_b V_b}{C^{3/2}}$$

$$C_{wk} \text{ is the wake blockage correction} = \frac{1 + 0.4 M^2}{\beta^2} \frac{C_D S}{4C}$$

The various terms of the corrections are defined below. For purposes of computation, the highest speed will be assumed so as to obtain the maximum correction. The radome and tower will be assumed to approximate the shape of a prolate spheroid plus an elliptical wing, each having a thickness ratio of unity.

The terms in the equations are evaluated as follows:

$$\beta = \sqrt{1 - M^2} = 0.964$$

where

$$M = .27$$

$$K_1 = \text{shape factor for tower} = 3.772$$

$$K_2 = \text{shape factor for sphere} = 1.329$$

$$T_w = \text{configuration factor for tower} = .855$$

$$T_b = \text{configuration factor for sphere} = .859$$

$$C = \text{tunnel cross-sectional area} = 96 \text{ ft.}^2$$

$$V_w = \text{volume of tower} = .852 \text{ ft.}^3$$

$$V_b = \text{volume of sphere} = .745 \text{ ft.}^3$$

$$C_D = \text{drag coefficient} = 0.25 \text{ (assumed)}$$

$$S = \text{model area} \approx 6.00 \text{ ft.}^2$$

Now inserting these values into the equations

$$K_w = .0015$$

$$K_b = .00101$$

$$K_{wk} = .00433$$

$$K = .00688$$

Substituting K into the corrections for M and q we get

$$\frac{M}{M_u} = 1.007$$

$$\frac{q}{q_u} = 1.014$$

Since the maximum correction is less than one per cent in Mach number and less than 1-1/2 per cent in dynamic pressure, wind tunnel corrections have been neglected for these tests.

C-7. Discussion

C-7a. General: The discussion and comments below are based primarily on the test results at 150 mph and one atmosphere, since this was the only condition for which the test data were extensively analyzed. However, examination of the uncorrected test data indicated relatively uniform characteristics and it is believed that the 150 mph. condition is representative of other test conditions. The test results are discussed in detail below. Design recommendations, based on the results of these tests, are given in Part II.

C-7b. Pressure Distribution: Of major interest is the difference in the pressure distribution over the surface of the radome. It is evident from the results of these tests that the tower base has a greater influence on the airflow over the radome than indicated by Ref. 1. Whereas it was originally expected that the influence on the airflow would be limited to the lower part of the radome, these tests show the influence to extend over the entire surface. The maximum negative pressures are higher than those predicted by potential flow around a sphere and peak pressures occur approximately 75 degrees aft of the stagnation point rather than 90 degrees. Also, the pressures on the lower part of the radome, where the influence of airflow around the base would be expected to be greatest, are lower, rather than higher, as originally estimated. Although these changes are relatively small they have a significant influence on the overall lift, drag and, especially on the distribution of load and stress in the envelope. These conditions are discussed in detail below:

C-7c. Lift: Lift loads were calculated using both strain gage values and pressure tap results obtained during tests. Good agreement was obtained between the two methods for both the total lift and for distribution of lift loads. Both the maximum and the total lift loads proved to be 25 to 30 percent higher than those calculated, using the classical pressure

distribution around a sphere (see Table I, page 21). The difference between the measured total lift and that calculated by the method recommended in Ref. 1 is even greater. The reason for this is that the Manual recommends a correction to account for higher negative pressure distribution over the bottom part of the envelope, whereas the wind tunnel test indicated lower values. The higher values shown in these tests appear to be reasonable and should be used as a basis for future designs.

C-7d. Drag: Similarly, the measurements of drag by pressure taps and strain gages showed good agreement and are about one-third higher than the drag predicted by the classical pressure distribution. However, the measured drag values are approximately 15 percent less than those based on the Manual (Ref. 1), as a correction had been included to account for added drag due to tower interference.

Even higher drag loads are predicted for the full scale radome based on the apparent increase in drag coefficient with Reynolds' number. This investigation is discussed more fully in paragraph C-4, but extrapolation of the test data indicates a drag coefficient of 0.81 as compared to .7, if based on Ref. 1. This 16 percent increase in drag load is probably conservative but, as this increase in drag coefficient at higher Reynolds' number is indicated by test, it is recommended that higher drag values be used in the design of large radomes.

C-7e. Shear: Ref. 1 Manual recommends that drag loads be transferred to the base as shear, using a sinusoidal distribution of shear load with the maximum value occurring at the 90 degree point. A sinusoidal shear distribution, using the total drag load based on classical pressure distribution over a sphere, is shown on Fig. 16. Shears measured on the 30 degree segments during wind tunnel tests closely approximate the sinusoidal distribution previously assumed, but are somewhat higher due to the higher drag loads. The exact distribution of shear load cannot be readily measured but, because of the close agreement indicated in Fig. 16, use of a sinusoidal distribution is recommended.

C-7f. Envelope Stress: The calculations based on wind tunnel test results indicate approximately a 6 percent increase in the maximum envelope stress N_{θ} over values calculated as recommended in the Manual, Ref. 1. However, because of the generally higher negative pressures acting on the surface of the radome and the higher drag loads, the calculated maximum value of N_{θ} is approximately 12 percent higher than the value as determined by the Manual.

It is interesting to note that the value of N_{θ} (representing the lift component of load) increased only 6 percent, while the total lift load increased approximately 45 percent. This difference is due to the change in pressure distribution which indicates that the peak loads are spread out over a much larger part of the radome, resulting in higher total loads with a relatively small increase in peak values. Although the N_{θ} is increased by a large percentage, this value is not critical for design. The resultant effect of the change in pressure distribution on envelope stresses is thus small.

C-7g. Effect of Terrain: The effect of installing the radome on a hilltop is to increase certain stresses in the envelope and attachment. However, the effect is small and does not apply to the maximum loads. Therefore, it is believed that this factor can be neglected in design.

C-7h. Effect of Reynolds' Number: Test results indicate a definite increase in drag coefficient at higher Reynolds' number. Although it is believed that the values obtained by extrapolating the test data are conservative, the higher values should be used in calculating maximum drag loads for large radomes.

P A R T II

RECOMMENDATIONS

A. Aerodynamic Loading of Radome

The pressure distribution determined in the wind tunnel tests carried out on this program is believed to represent more accurately the aerodynamic loading of a radome-tower unit similar to the AN/FPS-6 installation than the theoretical distribution given in Ref. 1 Manual. Therefore, it is recommended that the design loads for both the radome and tower be based on this new distribution. It is beyond the scope of this program to make corrections to the Manual to account fully for the influence of the modified pressure distribution on the radome and tower loads. It is recommended that a revised Radome Design Manual be issued to incorporate these modifications. However, in order to provide an interim basis for design of new equipment, correction factors are recommended herein.

B. Tower Loading

The tower loading from the radome results from both the aerodynamic loading on the radome envelope and the radome inflation pressure. The distribution of these loads depends primarily on the tower platform design. For example, if the tower platform is supported entirely from the outer columns of the tower, the platform loading due to dead weight and inflation pressure would be reacted at the sides of the platform and the resultant of aerodynamic and pressure loads on the columns would be reduced. On the other hand, with a platform design such as that employed on the FPS-6, which uses interior supporting columns in addition to the exterior columns, the majority of the dead weight and pressure loading may be supported by the interior columns and the resultant loading on the exterior columns would be increased. As the structural design of the towers varies widely between the different installations, no attempt has been made to suggest a detailed loading schedule. However, in order to provide data that will be helpful to the design engineer, maximum design load values are recommended and methods of applying these loads to the structure are suggested.

Another point of interest in the design of radome towers is that the peak lift and drag (shear) forces occur simultaneously in the same general area (75 to 90 degrees from stagnation point). However, as the stagnation point shifts with the wind and may occur at any point around the radome, the tower structure must be designed to support these peak loads with winds from any direction.

B-1. Lift Loads:

B-1a. The total lift, as determined from wind tunnel loads, was approximately 45 percent higher than values determined as outlined in

Ref. 1 Manual. It is recommended that, in calculating the loading for a radome of new design in accordance with the methods outlined in the Manual, values of K_L , given in Fig. 19, be increased by a factor of 1.45.

B-1b. The total lift load thus determined will be appreciably higher than that previously recommended. However, this value cannot be used directly in design as the distribution of load is not uniform around the periphery of the tower. The important design value is the maximum column loading. Based on the values determined with the balance system (Figs. 11a and 11b), it is recommended that each column be designed to support a load equal to 25 percent of the maximum lift load as calculated above. For design purposes, this load can be considered uniformly distributed over the 30 degree segment between columns or as a concentrated load for the design of the columns and their attachment to the platform.

B-2. Drag Loads (Shear):

B-2a. In order to account for the indicated increase in drag coefficient at higher Reynolds' number, it is recommended that, in calculating total drag load for new radar tower designs, the value of K_D (Ref. 1, Fig. 14) be increased by a factor of 1.16.

B-2b. Drag load is transferred into the tower as shear. Maximum shear values will, therefore, increase directly with the value of K_D (above). Maximum shear values at the base may therefore be calculated as recommended in Appendix I, Ref. 1, using the corrected value of K_D . The sinusoidal distribution of shear load recommended in Ref. 1 is believed to be representative of actual loading conditions.

B-2c. Because of the shear resistance of the tower platform, peak shear loads at the radome attachment can generally be considered to be distributed by the tower platform floor plates and reacted by the exterior column shear bracing or side panels in proportion to the relative stiffness of these members. (If interior column shear bracing is used, these members will also help carry drag load to the base of tower). This redistribution of load should be taken into account in designing the tower structure. Based on a sinusoidal distribution, it is recommended that the tower platform be designed so that a 30 degree segment of the tower structure can support approximately 15 percent of the total shear load.

B-2d. As the overturning moment at the tower platform is a direct function of the drag load, for design purposes the values of K_m (Ref. 1, Fig. 19) should also be increased by a factor of 1.16.

Note:

These values must be corrected by the reaction to dead weight and inflation pressure developed at the outer columns. This reaction will depend on the tower design as discussed in paragraph B, Part II.

B-3. Radome Attachment Loads

B-3a. As peak lift and shear loads occur simultaneously and at approximately the same point, the radome attachment must be designed to withstand these peak loads. The maximum vertical fabric load (pounds per inch - tangential to surface of envelope) is given by N_0 at the base (see Para. C, Part II).

B-3b. The peak shear value S is calculated as recommended in Appendix I, Ref. 1, using modified values of K_D (see Para. B-2a, Part II).

B-3c. The tower platform must be designed locally to resist and redistribute these peak attachment loads.

C. Envelope Stresses

Wind tunnel tests indicate a peak stress (N_0) only 6% higher than that calculated, as recommended in the Manual (Ref. 1). However, high stress occurs over a wider area of the radome. Peak longitudinal loads increase by a larger percentage but are not critical for design. It is therefore recommended that, for new designs, the maximum fabric load N_0 , calculated as recommended in the Manual (Ref. 1), be increased by a factor of 1.06. As this change is small, and as the Manual recommends a minimum factor of safety of three (3), no change is recommended in the material specification for radomes now in production, unless service experience indicates that a higher strength material is required.

D. Required Inflation Pressure

Wind tunnel tests indicate that inflation pressure is not critical with regard to pressure distribution or stability (for radome-tower configurations similar to the AN/FPS-6, using a two-ply, 45 degree bias constructed radome envelope). In order to keep envelope stresses to a minimum, it is therefore recommended that a minimum inflation pressure equal to "q" be used as a basis for design of the pressurization equipment, and that the maximum pressure be kept as low as possible. These values will permit a pressure variation of at least two inches of water, due to operational tolerances, without adversely affecting the stability of the radomes.

E. Effect of Terrain

As critical envelope stresses and tower loads are not increased when airflow is directed up over the radome at angles up to 30 degrees (simulating hilltop locations), this condition need not be considered in the design of the radome or tower.